HEAT TRANSFER THROUGH AN AIR CURTAIN

Thesis for the Degree of Ph. D.
MICHIGAN STATE UNIVERSITY

Gad Hetsroni

1963

This is to certify that the

thesis entitled

HEAT TRANSFER THROUGH AN AIR CURTAIN

presented by

Gad Hetsroni

has been accepted towards fulfillment
of the requirements for

Ph.D. degree in Agricultural Engineering

Carl W. Hall
Major professor

Date Jan. 21, 1963

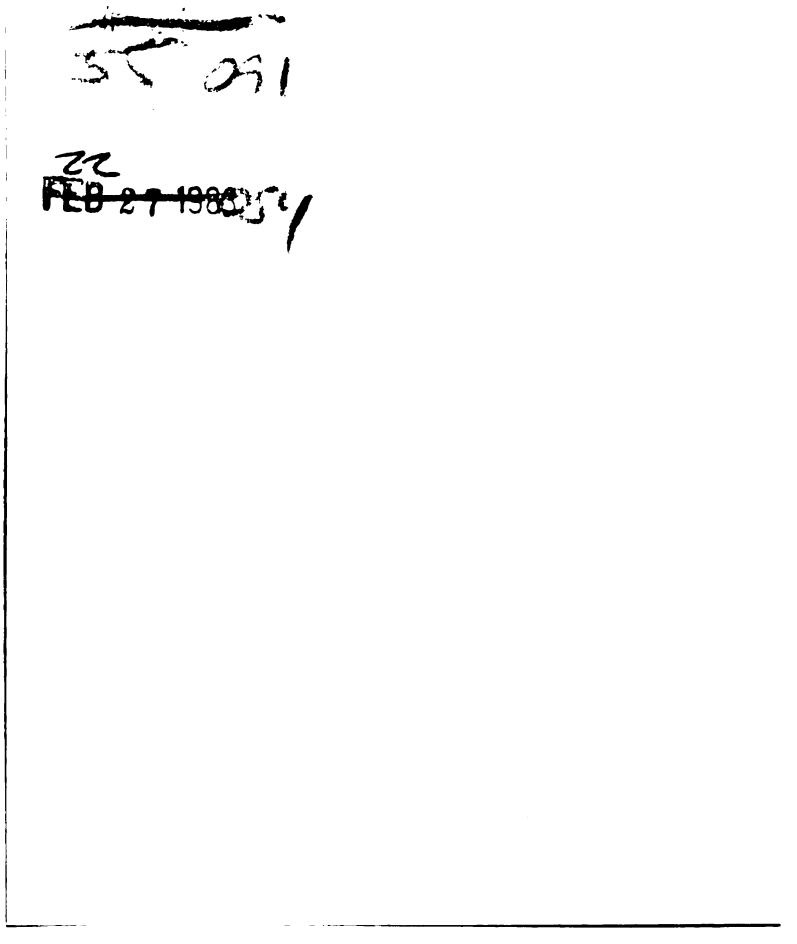

ABSTRACT

HEAT TRANSFER THROUGH AN AIR CURTAIN

by Gad Hetsroni

The air curtain studied here consists of a stream of air discharged downwards from nozzles above a doorway towards a return grille in the floor. The curtain of air insulates the interior from outside temperature, dust, fumes, insects, etc. It also provides an unrestricted and attractive doorway.

The fundamental heat transfer and flow characteristics of the air curtain were studied as dependent on the outlet air velocity and on the geometry of the curtain. A theoretical analysis was made, assuming that the air curtain is a two-dimensional jet. Semi-theoretical expressions for shear stress, stream function and eddy diffusivity were derived and plotted, based on an exponential type velocity profile, as suggested by Reichardt. A form of an error function was used for the temperature distribution in a two-dimensional jet.

A mechanism of heat transfer through the air curtain was suggested, based on the process of the air entrained and spilled by the jet. Based on this mechanism a functional relation was derived describing the heat transfer through an air curtain.

A two-dimensional air curtain was installed between two well-insulated chambers. The height of the curtain was varied from 5 to 7 ft., the outlet velocity from 9 to 35 ft. per sec. and the thickness from 0.115 to 0.340 ft. Velocity, temperature and turbulence distributions were measured, together with the quantities of heat transferred through the air curtain.

The exponential function for the velocity profile was confirmed experimentally. However, the coefficient in the exponent varied from the theoretical value for small aspect ratios and small outlet Reynolds numbers. The temperature profile based on the error function represented the data reasonably well. The coefficient in the error function was determined experimentally.

Hot wire anemometer studies revealed that the distribution of turbulence is asymmetrical around the centerline when a temperature gradient exists across the jet. The turbulence on the warm side of the jet was much higher than the turbulence on the cold side. The higher turbulence on the warm side caused a shift of the jet towards the cold side.

The semi-theoretical correlation for heat transfer through the air curtain is given by

$$St_0 = 0.0808 \sqrt{\frac{b_0}{H}}$$

where H is the height of the opening, $2b_0$ is the thickness of the air curtain at the outlet and St_0 is the Stanton number at the outlet nozzle. The above correlation was found to predict the heat transfer within ± 20 percent for the curtain parameter $\sqrt{\frac{b_0}{H}}$ between the values 0.090 to 0.170.

HEAT TRANSFER THROUGH AN AIR CURTAIN

By

Gad Hetsroni

A THESIS

Submitted to
Michigan State University
in partial fulfillment of the requirements
for the degree of

DOCTOR OF PHILOSOPHY

Department of Agricultural Engineering

1963

Carl W. Hall, Jan 21, 1963

ACKNOWLEDGEMENTS

The author wishes to express his sincere appreciation to Dr. Carl W. Hall (Agricultural Engineering), whose continued interest and encouragement made this investigation rewarding and enjoyable.

The guidance and unfailing assistance of Dr. A. M. Dhanak (Mechanical Engineering), who helped the author get some insight into the fields of heat transfer and fluid flow, are gratefully appreciated.

Thankful acknowledgement is extended to the other members of the guidance committee: Dr. D. H. Dewey (Horticulture), Dr. J. S. Frame (Mathematics), Dr. H. R. Henry and Dr. E. M. Laursen (Civil Engineering), for their helpful advice and suggestions.

The author is indebted to Dr. A. W. Farrall, chairman of the Department of Agricultural Engineering, for making available the graduate assistantship that made the undertaking of the investigation possible.

To the author's wife, Ruth, and daughter, Anath, whose unfailing love and devotion sustained the author throughout the challenges and frustrations of the graduate program; to them this manuscript is dedicated.

****

TABLE OF CONTENTS

LIST OF FIGURES

LIST OF FIGURES - Continued

LIST OF APPENDICES

NOMENCLATURE

a	width in the jet defined by equation (2.6.3), ft.
$a' =$	$a/\sqrt{2}\, C_m H'$
b	half the thickness of the air curtain, ft.
C_2	coefficient in the velocity distribution
C_m	velocity spreading coefficient defined by equation (2.1.33)
C_p	specific heat, Btu per lb, ^{o}F
C_T	temperature spreading coefficient defined in equation (2.5.5)
d	manometer head, in. manometer fluid
g	acceleration of free fall, ft per sq. sec.
h	coefficient of overall heat transfer, Btu per hr, ^{o}F sq. ft.
H	height of the door opening, ft.
H'	spill height, ft.
k	thermal conductivity, Btu per hr, ^{o}F, ft.
K	numerical coefficient in equation (2.6.17)
M	momentum flux, lb per ft, sq. sec.
q	sensible heat, Btu per hr.
Q	mass rate of flow, lb per sec.
t	temperature, ^{o}F
$T =$	$t - t_c$, $T_m = t_w - t_c$
u	velocity parallel to x- axis (longitudinal direction of the jet), ft. per sec.
v	velocity parallel to y - direction (transverse direction of the jet) ft. per sec.
x, y, z	rectangular coordinates
α	thermal diffusivity, sq. ft. per hr
β	dimensionless coefficient defined by equation (2.5.5)
γ_m	density of manometer fluid, lb_m per cu. ft.

$\delta = C_T / C_m$

ϵ apparent viscosity, sq. ft. per sec.

η dimensionless coefficient defined by equation (2.2.2)

θ time, hr

Λ proportionality function defined by equation (2.1.31)

μ dynamic viscosity, lb_m per ft. sec.

ν kinematic viscosity, sq. ft. per sec.

ρ density of air, lb_m per cu. ft.

τ shear stress, lb_m per ft. sq. sec.

ϕ functional relationship defined by equation (4.4.8)

ψ stream function

$St = h / \bar{u}_0 C_p \rho$, Stanton number

Bar above symbol indicates temporal mean

Primed symbol denotes a fluctuating component

The following subscript notation is also used

c	cold side of the air curtain
m	momentum
o	conditions at the outlet nozzle
T	temperature
w	warm side of the air curtain

1. INTRODUCTION

Cold storage areas should be as accessible as possible to workers. Air conditioned areas often have to be accessible to customers and the entrances should be as attractive as possible. Frequent opening of conventional doors causes air exchange inside the cooled (or heated) area. Where heavy traffic is encountered through such entrances, the air exchanges cause costly refrigeration losses. Large losses may prevent the refrigeration unit from maintaining a uniform and constant temperature.

Williams (1958) studied refrigeration losses through the door opening into cold rooms in a dairy plant. Under normal operating conditions for a 38°F room, losses through a 42 in. x 78 in. door ranged from 43,320 to 57,060 Btu per hr. Hukill (1946) estimated the losses through a 48 in. x 84 in. doorway into a 35°F room as 100,000 Btu per hr, plus the losses due to movement of water vapor into the cold storage.

An air curtain consists of a stream of air discharged from a series of nozzles above the entrance. The air is discharged downwards to a return grille in the floor. The air is then returned to the top nozzles through ductwork which contains filters, heating or cooling elements and fans.

Air curtains have gained popularity in department stores, banks, cold storages and other commercial buildings. A curtain of air insulates the doorway and eliminates many of the hazards and drawbacks of conventional doors by providing an attractive unrestricted opening. A curtain of air keeps air exchange to a minimum.

Additional advantages of open entrances sealed by an air curtain include: saving valuable floor space near entrance, eliminating door maintenance and repairs, and doorway accidents.

The concept of an air curtain is not new. A patent for a device to seal an entrance from outside weather by means of air flow was issued to T. Van Kennel in 1904 (U. S. Patent No. 774,730, Nov. 8, 1904). The Van Kennel curtain consisted of air streams introduced from both sides of an entrance. The air streams counteracted the wind forces blowing through the entrance. The idea had been successfully used in Switzerland and England prior to 1952. Since 1952 air curtains have also been used in this country. The largest known air curtain, 89 ft. wide, is at the entrance of Pan American's air terminal at Idlewild Airport, New York, and is described by Norton (1959).

There is little technical data presented in the literature concerning the relationships of air velocity, thickness of the curtain, temperature of air and rate of heat transfer. There is no reported information on the effect of turbulence on the heat transfer properties of an air curtain.

Cadiergues (1957) suggested a velocity limit of 33 ft. per sec. at head level for an air curtain. Air temperature at this level should be approximately 88°F. A discharge opening with a long slot is preferred. He recommended that the discharge air volume may vary from 1,500 to 15,000 cfm per linear foot of opening (he did not specify width of outlet).

Bjorkman (1961) recommends an outlet air velocity of 60 to 65 ft. per sec. for a curtain 18 ft. high. He also reports that air is spilled from the curtain starting at about 18 in. from the floor.

Michael (1960) recommends an air velocity less than 60 ft. per sec. at the outlet nozzle and about 12 ft. per sec. at the return grille.

Hetsroni (1961) found that the overall heat transfer coefficient through an air curtain varies from 5 to 16 Btu per hr. sq. ft. °F for an air curtain with a thickness of 0.97 to 1.81 ft. and for an average outlet velocity of 3 to 11 ft. per sec.

For an horizontal curtain Patchen (1961) suggests an air velocity of about 3.5 ft. per sec. at the outlet nozzle.

The work done to date presents data for some particular installations, rather than correlate basic relationships between the variables involved.

Future improvements in design will be based upon a knowledge of the basic information. Such information was sought in the present investigation.

2. THEORY

For the theoretical analysis the air curtain is handled as a two-dimensional jet. A commercial type air curtain is usually three-dimensional and is too complicated to lend itself to any theoretical calculation at this time. After the basic heat transfer mechanism through a two-dimensional curtain is understood it may be extrapolated to three-dimensional cases.

There are three well defined regions in a two-dimensional jet. The non-turbulent core is a triangular shaped region that has its base on the nozzle opening and is about 5 nozzle widths long ($x_0 = 10\ b_0$). In this region the intensity of the turbulence is low and the velocity is substantially uniform and equals the discharge velocity ($\bar{u}_o$). Surrounding this core is a transition zone which extends to about 10 nozzle widths from the nozzle. In the region of flow over a distance of more than 10 nozzle widths from the nozzle the flow is fully developed. The relative intensity of turbulence is rather high.

Before any further analysis is carried on, a few basic assumptions have to be stated namely:

a) The pressure is hydrostatically distributed throughout the flow, i.e., the pressure gradient in the zone of established flow is negligible.

b) The diffusion process is dynamically similar under all conditions, i.e., the velocity profiles at various distances along the jet are affine.

c) The turbulent effect is considerably larger than the molecular effects.

d) The flow is incompressible and the temperature difference between the cold and warm sections of the jet is small so that essentially the density is constant.

The first and second assumptions are well established. Liepmann (1947), Hinze (1949), Albertson (1950), Alexander (1953), Pai (1954) and many others have been using these assumptions as a basis for their analysis and reported them to be satisfactory.

The third assumption is used mainly in computations of turbulence. Again it is well recognized and accepted for cases like free-turbulent-shear flow.

The last assumption is an approximation of the case at hand, to facilitate the mathematical handling. When the temperature gradient across the jet is about $50^{\circ}F$, the density of the air varies by less than ten percent. Usually the temperature gradient is smaller and the approximation that the density is constant is even better.

2.1 Basic equations and background.

The equation of motion for a two dimensional flow can be written as

$$\rho\left(\frac{\partial u}{\partial \theta} + u\frac{\partial u}{\partial x} + v\frac{\partial u}{\partial y}\right) = -\frac{\partial p}{\partial x} + \mu\left(\frac{\partial^2 u}{\partial x^2} + \frac{\partial^2 u}{\partial y^2}\right) \qquad (2.1.1)$$

$$\rho\left(\frac{\partial v}{\partial \theta} + u\frac{\partial v}{\partial x} + v\frac{\partial v}{\partial y}\right) = -\frac{\partial p}{\partial y} + \mu\left(\frac{\partial^2 v}{\partial x^2} + \frac{\partial^2 v}{\partial y^2}\right) \qquad (2.1.2)$$

Making estimates of the order of magnitude of the terms it is found that for a steady state turbulent flow in a boundary layer, Prandtl's approximations of Reynolds' equation apply, namely

$$\rho\left(\bar{u}\frac{\partial \bar{u}}{\partial x} + \bar{v}\frac{\partial \bar{u}}{\partial y}\right) = -\frac{\partial p}{\partial x} + \frac{\partial \tau}{\partial y} \qquad (2.1.3)$$

and

$$\frac{\partial p}{\partial y} = 0 \qquad (2.1.4)$$

where $$\tau = \mu \frac{\partial \bar{u}}{\partial y} - \rho \overline{u'v'} \qquad (2.1.5)$$

and where the bars over the symbols indicate temporal mean values.

The equation of energy can be written as

$$\rho C_p \left(\frac{\partial T}{\partial \theta} + u \frac{\partial T}{\partial x} + v \frac{\partial T}{\partial y}\right) = k \left(\frac{\partial^2 T}{\partial x^2} + \frac{\partial^2 T}{\partial y^2}\right) \qquad (2.1.6)$$

which simplifies, with same approximations as before to read as follows:

$$\bar{u} \frac{\partial \bar{T}}{\partial x} + \bar{v} \frac{\partial \bar{T}}{\partial y} = \frac{k}{\rho C_p} \frac{\partial^2 \bar{T}}{\partial y^2} \qquad (2.1.7)$$

In addition to the equation of motion and the equation of energy, the equation of continuity must apply:

$$\frac{\partial(\rho \bar{u})}{\partial x} + \frac{\partial(\rho \bar{v})}{\partial y} = 0 \qquad (2.1.8)$$

The boundary conditions for the equation of motion are

$$\text{at} \quad y = 0, \qquad v = 0, \qquad \tau = 0 \qquad (2.1.9a)$$

$$\text{at} \quad y = \infty, \qquad u = 0, \qquad \tau = 0 \qquad (2.1.9b)$$

Multiplying equation (2.1.8) by $\bar{u}$ and adding to equation (2.1.3) results in

$$\frac{\partial(\rho \bar{u}^2)}{\partial x} + \frac{\partial(\rho \bar{u}\bar{v})}{\partial y} = -\frac{\partial p}{\partial x} + \frac{\partial \tau}{\partial y} \qquad (2.1.10)$$

Integrating equation (2.1.10) between two variable limits a(x) and b(x) one obtains:

$$\int_a^b \frac{\partial}{\partial x} (\rho \bar{u}^2) dy = \tau_b - \tau_a - \rho \bar{u} \bar{v} \Big|_a^b - \int_a^b \frac{\partial p}{\partial x} dy \qquad (2.1.11)$$

Letting a = 0 and b = ∞ and applying the first postulate, namely $\frac{\partial p}{\partial x} = 0$, together with the boundary conditions of equation (2.1.9) one gets

$$\frac{d}{dx} \int_0^\infty \rho \bar{u}^2 \, dy = 0 \qquad (2.1.12)$$

where it was assumed that the order of integration and differentiation is immaterial.

From equation (2.1.12) it is evident that:

$$\int_0^{\infty} \rho \, \bar{u}^2 \, dy = M = \text{constant} \qquad (2.1.13)$$

where M is the momentum flux per unit width of the jet. Equation (2.1.13) states the constancy of momentum flux at every cross section of a two-dimensional jet.

The second postulate states that the velocity profiles in the zone of established flow are affine. In other words the rate of spread of the profiles must be linear, progressing away from the outlet nozzle, or

$$\frac{\bar{u}}{\bar{u}_m} = f(\eta) \qquad (2.1.14)$$

where

$$\eta = \eta\left(\frac{y}{x}\right) \qquad (2.1.15)$$

Forming a ratio of momentum flux at some distance x from the outlet to the momentum flux at the outlet, assuming that the density is constant, and substituting equation (2.1.14) one gets:

$$\frac{M}{M_0} = 1 = \frac{\int_0^{\infty} x \, \bar{u}_m^2 \, f^2(\eta) d\eta}{\bar{u}_0^2 \, b_0} = \left(\frac{\bar{u}_m}{\bar{u}_0}\right)^2 \frac{I_m x}{b_0} \qquad (2.1.16)$$

where

$$I_m = \int_0^{\infty} f^2(\eta) \, d\eta \qquad (2.1.17)$$

The same ratio can be written for the zone of establishment, assuming that the functional relationship of equation (2.1.14) holds true in this region,

$$\frac{M}{M_0} = 1 = \frac{\int_0^{b} \bar{u}_0^2 dy + \int_b^{\infty} x \, \bar{u}_m^2 \, f^2(\eta) \, d\eta}{\bar{u}_0^2 \, b_0} = \frac{x_0 \, I_m}{b_0} \qquad (2.1.18)$$

From which I_m can be determined and substituted back into equation (2.1.16) giving:

$$\frac{\bar{u}_m}{u_0} = \sqrt{\frac{x_0}{x}} \qquad (2.1.19)$$

where x_0 is the length of the irrotational core. This computation was suggested by Corrsin (1950) and Albertson et al. (1950). The length of the irrotational core was also determined experimentally by the same authors. The length of the irrotational core for a three-dimensional jet was reported by Corrsin (1950) to be 7d to 8d (where d is the outlet diameter). Albertson et al. (1950) report that for a two-dimensional jet $x_0 = 10.4\, b_0$, and $x_0 = 6.2d$ for the three-dimensional case.

Since there exists at the present time no satisfactory theory of turbulent flow some assumptions pertaining to the nature of the flow have to be made.

The theories providing for such assumption, are based on either statistical mechanics or on phenomenological theories, substantiated by experimentation.

The statistical approach was first used by Taylor (1935). Taylor based his theory on the assumption that the vorticity is conserved. However, no further progress could be made without introducing further simplifying assumptions. One such assumption is that the components of vorticity are transported unchanged by the turbulence. This is a drastic assumption and is clearly untrue for most cases, as was recognized by Taylor himself. Howarth (1938) carried forward Taylor's theory by introducing an apparent eddy viscosity, assuming that turbulence is isotropic and that the momentum is conserved during the mixing process. Taylor's theory clearly suffers from the necessity to make quite drastic assumptions, which were not confirmed experimentally.

The limitations of Taylor's theory are pointed out by Liepmann (1947), Alexander (1953) and others.

The phenomenological theories of turbulent shear flow date back to Saint-Venant (1843) who introduced the mixing coefficient ϵ. It was realized by Saint-Venant that ϵ is not a constant throughout the flow and is dependent on the scale and intensity of turbulent fluctuations.

Boussinesq (1877) suggested the coefficient ϵ_m for momentum transfer by turbulence. The equation of motion thus becomes

$$u \frac{\partial u}{\partial x} + v \frac{\partial u}{\partial y} = \frac{\partial}{\partial y} \left(\epsilon_m \frac{\partial u}{\partial y} \right) \qquad (2.1.20)$$

For a flow in a pipe ϵ_m was supposed to be a function only of the Reynolds number, but was also found to be a complicated function of the location. Hinze (1948) felt that Boussinesq's hypothesis may apply to free jets. Hinze evaluated the apparent eddy viscosity and found

$$\epsilon_m = 0.00196(x + a)\, u_m \qquad (2.1.21)$$

where "a" is the distance from the outlet nozzle to an equivalent point source. Hinze also introduced a coefficient ϵ_Γ for apparent concentration and temperature transfer by turbulence, such that the energy equation is

$$u \frac{\partial \Gamma}{\partial x} + v \frac{\partial \Gamma}{\partial y} = \frac{\partial}{\partial y} \left(\epsilon_\Gamma \frac{\partial \Gamma}{\partial y} \right) \qquad (2.1.22)$$

The ratio between ϵ_Γ and ϵ_m is inversely proportional to the distance from the nozzle x. He found this ratio to be a rather complicated function of location and velocity, with a large number of empirical constants.

The concept of mixing length was introduced by Prandtl (1925) and his school. Prandtl postulated that as the masses of fluid migrated laterally they carried with them the momentum concentration of their point of origin. A typical velocity fluctuation u' due to such migration

is characterized by

$$u' \propto l \frac{\partial \bar{u}}{\partial y} \tag{2.1.23}$$

where l is the mixing length.
If it is further assumed that

$$v' \propto u' \tag{2.1.24}$$

then the shear is given by

$$\tau = \rho \, l^2 \left| \frac{\partial \bar{u}}{\partial y} \right| \frac{\partial \bar{u}}{\partial y} \tag{2.1.25}$$

If it is now assumed that the mixing length is proportional to the distance from the outlet

$$l = c_1 x \tag{2.1.26}$$

then Prandtl's assumption leads to useful results because the stream function for the flow can be obtained:

$$\Psi = x F \left(\frac{y}{x} \right) \tag{2.1.27}$$

The virtual kinematic viscosity (eddy viscosity), as resulting from Prandtl's hypothesis is

$$\epsilon = \chi_1 b \frac{\partial u}{\partial y} \tag{2.1.28}$$

where χ_1 denotes a dimensionless constant, to be determined experimentally.

Prandtl's theory was extended by Howarth (1938) to include heat and mass transfer. Howarth suggested that the temperature distribution is similar to velocity distribution. However, Hinze (1948), Forstall (1950),

and others measured the temperature and velocity distributions in a free jet and found that they are not equal. The discrepancy was large enough to require a new theory.

An empirical approach to the problem of free turbulence was suggested by Reichardt (1941). Reichardt noticed a similarity between the turbulent process and molecular phenomena of thermal conduction. Even though in their details the molecular and molar processes differ, it is highly probable that with the turbulent processes also, purely statistical distribution will be obtained. In fact, the measured velocity distribution in free jets exhibits a strong similarity to the Gauss error curve. The hypothesis that the distribution of turbulent momentum of the principle motion is capable of being represented by a partial differential equation of the type of the equation of thermal conductivity (the location parameter appearing in place of the time parameter), can be put:

$$\frac{\partial \overline{u}^2}{\partial x} = \Lambda \frac{\partial^2 \overline{u}^2}{\partial y^2} \qquad (2.1.29)$$

The solution to equation (2.1.29) is

$$\overline{u}^2 = C_1 + \frac{C_2}{b} \exp-\left(\frac{y}{b} \right)^2 \qquad (2.1.30)$$

if the "transmission quantity" Λ is

$$\Lambda = \frac{b}{2} \frac{db}{dx} \qquad (2.1.31)$$

where b=b(x) is a measure for the width of the mixing zone, and C_1 and C_2 are constants.

Equation (2.1.30) may be put in a similar form

$$\overline{u} = \overline{u}_m \exp-\left(\frac{y}{\sqrt{2}\,\sigma} \right)^2 \qquad (2.1.32)$$

where

$$\sigma = C_m x \qquad (2.1.33)$$

which has been found by Albertson (1950), Reichardt (1951), Alexander (1953) and others to be in substantial agreement with experimental observation.

In summarizing, there exists at the present time no satisfactory theory of turbulent flow. The concept of simple mixing length is not usable and does not agree with the experiments. The assumption of constant exchange coefficient by Prandtl and Görtler does not agree with measured values, as pointed out by Liepmann (1947). The previous theories have been successful in predicting mean-velocity distribution which agrees well with experiments because any reasonable assumption regarding the dependence of u' on the mean flow parameters, results in a solution which fits the data reasonably well. This, however, is not at all a proof that the assumptions of the theory are correct. As Corrsin (1949) mentioned, it does not seem possible to differentiate among these theories on the basis of mean flow measurements made with a total-head-impact-tube.

Since most parts of these studies deal with temporal mean velocities, the velocity distribution as suggested by Reichardt was chosen. This distribution involves the fewest objectionable assumptions and offers the easiest mathematical handling. Several researchers have used this approach and their results are very satisfactory.

2.2 Velocity.

Making use of Reichardt's theory the velocity distribution is as follows:

$$\frac{\bar{u}}{u_m} = \exp(-\eta^2) \qquad (2.2.1)$$

where

$$\eta = \frac{y}{\sqrt{2}\, C_m x} \qquad (2.2.2)$$

Forming the ratio of momentum flux at any distance x from the outlet to the momentum flux at the outlet, using equation (2.2.1) one gets

$$\frac{M}{M_0} = 1 = \frac{\int_0^\infty \bar{u}^2 \, dy}{\bar{u}_0^2 \, b_0} = \frac{\bar{u}_m^2 \int_0^\infty \exp(-\eta^2) \, dy}{\bar{u}_0^2 \, b_0} \qquad (2.2.3)$$

After performing the integration and simplifying one gets

$$\frac{\bar{u}_m}{\bar{u}_0} = \sqrt{\frac{2 \, b_0}{\sqrt{\pi} \, C_m x}} \qquad (2.2.4)$$

Substitution of equation (2.2.4) into equation (2.2.1) yields

$$\frac{\bar{u}}{\bar{u}_0} = \sqrt{\frac{2 \, b_0}{\sqrt{\pi} \, C_m x}} \exp - \left(\frac{y}{\sqrt{2} \, C_m x} \right)^2 \qquad (2.2.5)$$

which gives the temporal mean velocity at any point as a function of the outlet velocity, of the location, of the geometry and of a numerical constant C_m.

The constant C_m was determined by Albertson et al. (1950) for a two-dimensional jet issued into an infinite medium. Albertson gives

$$C_m = 0.109 \qquad (2.2.6)$$

In order to determine the transverse velocity the equation of continuity will be integrated with respect to y,

$$\bar{v} = - \int_0^y \frac{\partial \bar{u}}{\partial x} \, dy \qquad (2.2.7)$$

Differentiation of equation (2.2.5) with respect to x and substitution into equation (2.2.7) yields, after a change of variables

$$\bar{v} = \frac{A\,\bar{u}_0 C_m \sqrt{\pi}}{2\sqrt{2}} \frac{2}{\sqrt{\pi}} \int_0^{\eta} [\exp(-\eta^2) - 4\eta^2 \exp(-\eta^2)]d\eta$$

where
$$A \equiv \sqrt{\frac{2b_0}{\sqrt{\pi}\, C_m x}} \qquad (2.2.8)$$

the first part of the integral is recognized as the error function of η, and the second part can be integrated by parts.

Finally

$$\bar{v} = \sqrt{2}\, C_m\, A\, \bar{u}_0 \left[\eta \exp(-\eta^2) - \frac{\sqrt{\pi}}{4} \operatorname{erf}(\eta)\right] \qquad (2.2.9)$$

In addition the stream function can be determined from equation (2.2.5). The stream function Ψ is defined by

$$u = \frac{\partial \Psi}{\partial y}, \quad v = -\frac{\partial \Psi}{\partial x} \qquad (2.2.10)$$

Substituting equation (2.2.5) into equation (2.2.10) and integrating, one obtains

$$\Psi = \int_0^y u\,dy = \sqrt{2}\, C_m x \int_0^{\eta} \bar{u}_0\, A \exp(-\eta^2)\, d\eta$$

or

$$\Psi = \sqrt{\sqrt{\pi}\, b_0 C_m x}\ \bar{u}_0 \operatorname{erf}(\eta) \qquad (2.2.11)$$

which clearly satisfies equations (2.2.10).

In Appendix A it is shown that equations (2.2.1) and (2.2.9) together with expression for the shear τ satisfy the equation of motion.

2.3 Shear Stress.

For a two-dimensional turbulent flow, the boundary layer approximation of the equation of motion can be written as

$$\rho\left(\bar{u}\frac{\partial \bar{u}}{\partial x} + \bar{v}\frac{\partial \bar{u}}{\partial y}\right) = -\frac{\partial \bar{p}}{\partial x} + \frac{\partial}{\partial y}\left(\mu\frac{\partial \bar{u}}{\partial y} - \rho\,\overline{u'v'}\right) \qquad (2.3.1)$$

where the bar over the symbols indicates temporal mean and the prime indicates a deviation from that mean.

The second term on the right hand side is the derivative of the shear stress τ ,

$$\tau = \mu \frac{\partial \bar{u}}{\partial y} - \rho \overline{u'v'} \qquad (2.3.2)$$

However, in highly turbulent flow the first term on the right hand side of equation (2.3.2) is usually much smaller than the second term, and can therefore be neglected, hence

$$\tau = - \rho \overline{u'v'} \qquad (2.3.3)$$

The shear stress can be determined theoretically from equation (2.3.1) by simple integration with respect to y. Performing the integration, keeping in mind the first postulate, i.e., $\frac{\partial p}{\partial x} = 0$, one obtains:

$$\tau = \rho \int_0^y (\bar{u} \frac{\partial \bar{u}}{\partial x} + \bar{v} \frac{\partial \bar{u}}{\partial y}) \, dy \qquad (2.3.4)$$

Substitution for the velocities and their derivatives from the previous paragraph gives:

$$\tau = \rho \int_0^y \left\{ \bar{u}_0 A \exp(-\eta^2) \frac{A\bar{u}_0}{2x} \exp(-\eta^2)(4\eta^2-1) - A\bar{u}_0 C_m \sqrt{2} [\eta \exp(-\eta^2) - \frac{\sqrt{\pi}}{4} \operatorname{erf}(\eta)] \frac{\sqrt{2}\, \bar{u}_0 A \eta}{C_m x} \exp(-\eta^2) \right\} dy \qquad (2.3.5)$$

changing variables and simplifying:

$$\tau = \frac{\rho C_m \bar{u}_0^2 A^2}{\sqrt{2}} \left\{ - \frac{1}{\sqrt{2}} \int_0^{\eta} \exp(-2\eta^2) d(\sqrt{2}\,\eta) + 2 \int_0^{\eta} \eta \exp(-\eta^2) \frac{\sqrt{\pi}}{2} \operatorname{erf}(\eta) d\eta \right.$$

The first integral is recognized as the error function of η and the second integral can be integrated by parts:

$$\int_0^{\eta} [2\eta \exp(-\eta^2) \frac{\sqrt{\pi}}{2} \operatorname{erf}(\eta)]d\eta = -\frac{\sqrt{\pi}}{2} \exp(-\eta^2) \operatorname{erf}(\eta) + \sqrt{\frac{\pi}{8}} \operatorname{erf}(\eta) \quad (2.3.6)$$

The shear stress is, therefore

$$\tau = -\frac{\rho C_m \sqrt{\pi}\, \bar{u}_0^2 A^2}{2\sqrt{2}} \exp(-\eta^2) \operatorname{erf}(\eta)$$

or

$$\tau = -\frac{\rho \bar{u}_0^2 b_0}{\sqrt{2}\, x} \exp(-\eta^2) \operatorname{erf}(\eta) \quad (2.3.7)$$

Using Boussinesq's coefficient ϵ_m for the momentum transfer by turbulence, i.e.,

$$\tau = \epsilon_m \frac{\partial \bar{u}}{\partial y} \quad (2.3.8)$$

one can determine ϵ_m by combining equation (2.3.8) and the derivative of equation (2.2.5), i.e.,

$$\tau = \epsilon_m \frac{\partial \bar{u}}{\partial y} = -\epsilon_m \frac{2 \bar{u}_0 A \eta^2}{y} \exp(-\eta^2) \quad (2.3.9)$$

combining this equation with equation (2.3.7) one obtains:

$$\epsilon_m = \frac{\bar{u}_0 b_0 C_m}{2\eta A} \operatorname{erf}(\eta) \quad (2.3.10)$$

It should be noticed that both τ and ϵ_m are functions of the location, of the outlet velocity and of the geometry.

In a dimensionless form equation (2.3.10) can be written as:

$$\frac{\epsilon_m}{\nu} = \mathrm{Re} \sqrt{\frac{C_m^3 \sqrt{\pi}\, x}{8 b_0}} \frac{\operatorname{erf}(\eta)}{\eta} \quad (2.3.11)$$

and consideration of the order of magnitude of the terms show that for $\eta < 10^3$

$$\frac{\epsilon_m}{\nu} << 1$$

which verifies the assumption previously made.

In Appendix A it is shown that equation (2.3.7), together with expressions for velocity previously obtained, satisfies the equation of motion.

2.4 Mass Rate of Flow.

The mass rate of flow through any cross section of a two-dimensional jet can be obtained by integrating the velocity profile with respect to y. For a unit width, one gets:

$$Q = 2 \int_0^\infty \rho \, \bar{u} \, dy \qquad (2.4.1)$$

Forming a ratio of the mass rate of flow at some distance x from the outlet (Q) to the mass rate of flow at the outlet nozzle (Q_0):

$$\frac{Q}{Q_0} = \frac{\int_0^\infty \rho \, \bar{u} \, dy}{\rho_0 \, \bar{u}_0 \, b_0} \qquad (2.4.2)$$

Using the fourth postulate, i.e., that the density is essentially constant, the above equation simplifies to

$$\frac{Q}{Q_0} = \frac{\int_0^\infty \bar{u} \, dy}{\bar{u}_0 \, b_0} \qquad (2.4.3)$$

and since $$\frac{\bar{u}}{\bar{u}_m} = f(\eta) \qquad (2.1.11)$$

one gets $$\frac{Q}{Q_0} = \frac{\int_0^\infty x \, \bar{u}_m f(\eta) d\eta}{\bar{u}_0 \, b_0} \qquad (2.4.4)$$

but $$\bar{u}_m = u_0 \sqrt{\frac{x_0}{x}} \qquad (2.1.16)$$

and since $$x_0 = \frac{b_0}{I_m} \qquad (2.1.15)$$

equation (2.4.4) becomes

$$\frac{Q}{Q_0} = \frac{\int_0^{\infty} \bar{u}_0 \sqrt{\frac{x}{b_0 I_m}}\, f(\eta) d\eta}{\bar{u}_c}$$

or

$$\frac{Q}{Q_0} = \sqrt{\frac{x}{b_0} \frac{Iq^2}{I_m}} \qquad (2.4.5)$$

where

$$Iq = \int_0^{\infty} f(\eta)\, d\eta \qquad (2.4.6)$$

In order to advance the study beyond a merely functional relationship the velocity profile of equation (2.2.5) is substituted in equation (2.4.3) to obtain:

$$\frac{Q}{Q_0} = \frac{\int_0^{\infty} \bar{u}_0 A \exp(-\eta^2)\, dy}{\bar{u}_0 b_0} \qquad (2.4.7)$$

After change of variables and some simplification the ratio of mass rate of flow is found:

$$\frac{Q}{Q_0} = \sqrt{\frac{\sqrt{\pi} C_m x}{b_0}} \qquad (2.4.8)$$

and when equation (2.2.6) is substituted for C_m

$$\frac{Q}{Q_0} = 0.438 \sqrt{\frac{x}{b_0}} \qquad (2.4.9)$$

It should be noted from the above equation that the mass rate of flow is proportional to the square root of the distance from the outlet nozzle, i.e., air is entrained into the jet from the two sides. This fact was confirmed experimentally by Albertson (1950). For a three-dimensional coaxial jet similar analysis yields

$$\frac{Q}{Q_0} = 0.32 \frac{x}{d_0} \qquad (2.4.10)$$

for air jet issued into air as medium. This result was also confirmed by Ricou (1961).

2.5 Temperature.

The process of turbulent mixing causes the transfer of properties of fluid in a lateral direction of the stream.

According to Prandtl's mixing length theory the mechanisms of transfer of momentum and heat in free turbulent flow are identical, which means that the temperature profile should be identical to the velocity profile. However, measurements by Reichardt (1942) in a two-dimensional jet show that temperature profile is wider than velocity profile. This result has been confirmed by Corrsin (1950), Hinze (1948) and Forstall (1950), for a three-dimensional jet. These results agree with Taylor's theory, discussed previously, that turbulent mixing motion causes an exchange of vorticity rather than momentum.

The question as to why momentum should transfer less rapidly than temperature, even though in all qualitative aspects there are remarkable similarities among the turbulent transport of these two properties, has yet to be answered. The explanation that temperature, being a scalar quantity, is more readily transported than momentum, a vector, is not quite satisfactory.

A remarkable relation between the temperature and velocity distributions was derived by Reichardt (1944), based on theoretical and empirical argument. Reichardt gives

$$\frac{\overline{T}}{\overline{T}_m} = \exp\left(-\frac{y^2}{2 C_T^2 x^2}\right) \qquad (2.5.1)$$

or

$$\frac{\overline{T}}{\overline{T}_m} = \left(\frac{u}{u_m}\right)^{\delta} \qquad (2.5.2)$$

where

$$\delta = \frac{C_T}{C_m} \qquad (2.5.3)$$

For a two-dimensional jet his results show $\delta = \sqrt{2}$.

Forstall (1950) suggests that for a three-dimensional coaxial jet the ratio of momentum transport to temperature transport is a constant 0.7.

There is no information in the literature concerning temperature profile in a two-dimensional jet with a temperature gradient across it. Nevertheless the mechanism of heat transport in a turbulent jet, under these conditions, should be similar to that of a jet issued into a medium of different temperature. Therefore, the functional relationship should hold, even though it might have a different form.

An integral of equation (2.5.1) is such a relationship and it is therefore suggested, pending experimental confirmation later, that for a two-dimensional jet with a temperature gradient across it, the temperature profile has the assumed form

$$\frac{\overline{T}}{\overline{T}_m} = \tfrac{1}{2}\left[\, 1 + \operatorname{erf}(\beta)\right] \qquad (2.5.4)$$

where

$$\beta = \frac{y}{\sqrt{2}\, C_T x} \qquad (2.5.5)$$

and

$$\overline{T} = \overline{t} - \overline{t}_c \quad ; \quad \overline{T}_m = \overline{t}_w - \overline{t}_c \qquad (2.5.6)$$

with the boundary conditions

$$\begin{aligned} &\text{at} \quad y = -\infty \;, \quad T = 0 \\ &\text{at} \quad y = +\infty \;, \quad T = 1 \end{aligned} \qquad (2.5.7)$$

2.6 Heat Transfer Through an Air Curtain.

In section 2.4 it was shown that the mass rate of flow in a two-dimentional jet is increasing proportionally to the square root of the distance from the outlet nozzle, i.e.,

$$Q \propto x^{\frac{1}{2}} \qquad (2.6.1)$$

Namely, as the jet is progressing away from the outlet nozzle air is entrained into it from both sides. When a temperature gradient is maintained across the jet the temperature of the entrained air from the cold side is t_c and the temperature of the entrained air from the warm side is t_w. Due to the turbulence the heat is transferred from one side of the jet to the other and a temperature profile is established, given by equation (2.5.4).

At the floor level a mass rate of flow Q_0 is drawn into the return grille, corresponding to the mass rate of flow at the outlet nozzle (providing the ductwork from the return grille to the outlet nozzle is a closed system). Since the mass rate of flow is increasing as the square root of the distance from the outlet, and then is decreased near the return grille, it has to reach a maximum (Q_m) at some distance H' from the outlet nozzle. The mass rate of flow which is entrained into the jet is spilled out to both the cold and the warm sides of the curtain. The mass of air spilled into the cold side at the spill height H' is given by

$$Q_s = \tfrac{1}{2} (Q_m - Q_0) \qquad (2.6.2)$$

for a symmetrical jet.

At the distance H' from the outlet nozzle there must exist two points "-a" and "+a" such that

$$Q_0 = \int_{-a}^{+a} \rho \bar{u} \, dy \qquad \text{at } x = H' \qquad (2.6.3)$$

where points "a" are assumed to be symmetrical about the centerline of the jet.

The quantity of heat (q) which is carried into the cold side with the spilled air is the major part of the heat transferred through the air curtain. Therefore it is suggested that the entrainment-spill mechanism is the main heat transfer mechanism, at a certain velocity range.

The spill mechanism itself is evidently highly complex and difficult to analyze. Hence the entrainment - spill model suggested here will be simplified, as outlined below. This simplification is necessary in order to get a heat transfer correlation.

The quantity of heat carried with the spilled air into the cold side can be calculated by multiplying the ordinates in the velocity profile by the corresponding ordinates in the temperature profile, and integrating the product from "a" to infinity, with respect to y,

$$q = \int_a^{\infty} \rho\, C_p\, \bar{u}\, \bar{T}\, dy \qquad (2.6.4)$$

where q is the quantity of heat, in Btu per hr. per unit width, carried into the cold side by the spilled air.

In previous sections the expressions for the velocity and the temperature were obtained:

$$\bar{T} = \bar{T}_m * \tfrac{1}{2} [\, 1 + \text{erf}\, (\beta)] \qquad (2.6.5)$$

and

$$\bar{u} = \bar{u}_0\, A \exp(-\eta^2) \qquad (2.6.6)$$

Substitution of equations (2.6.5) and (2.6.6) into equation (2.6.4) yields

$$q = \rho\, C_p\, \bar{u}_0\, \bar{T}_m\, A\, \tfrac{1}{2} \int_a^{\infty} \exp(-\eta^2) [1 + \text{erf}\, (\beta)]\, dy \qquad (2.6.7)$$

upon changing variables and simplifying one gets

$$q = \rho\, C_p\, \bar{u}_0\, \bar{T}_m \sqrt{\frac{C_m H' b_0}{\sqrt{\pi}}} \int_{a'}^{\infty} \exp(-\eta^2) [1 + \text{erf}\, (\beta)]\, d\eta \qquad (2.6.8)$$

where

$$a' = \frac{a}{\sqrt{2}\, C_m\, H'} \qquad (2.6.9)$$

The overall heat transfer coefficient is defined as

$$h = \frac{q}{H\, \bar{T}_m} \qquad (2.6.10)$$

Combination of equations (2.6.8) and (2.6.10) results in the expression

$$h = \rho\, C_p\, \bar{u}_0\, \frac{\sqrt{b_0 H'}}{H}\, \sqrt{\frac{C_m}{\sqrt{\pi}}} \int_{a'}^{\infty} \exp(-\eta^2)\left[1 + \operatorname{erf}\left(\frac{\eta}{\delta}\right)\right] d\eta \qquad (2.6.11)$$

where $$\beta = \frac{\eta}{\delta}$$

was substituted.

In dimensionless form equation (2.6.11) can be written:

$$\frac{Nu}{Pr} = f(a')\, Re \sqrt{\frac{H'}{b_0}} \qquad (2.6.12)$$

where the Nusselt number is $$Nu = \frac{hH}{k} \qquad (2.6.13)$$

the Prandtl number is $$Pr = \frac{\nu}{a} \qquad (2.6.14)$$

The Reynolds number is $$Re = \frac{\bar{u}_0\, b_0}{\nu} \qquad (2.6.15)$$

and the function f(a') is given by

$$f(a') = \sqrt{\frac{C_m}{\sqrt{\pi}}} \int_{a'}^{\infty} \exp(-\eta^2)\left[1 + \operatorname{erf}\left(\frac{\eta}{\delta}\right)\right] d\eta \qquad (2.6.16)$$

In view of the fact that the spill height H' is generally not known, equation (2.6.12) will now be changed into the form:

$$\frac{Nu}{Pr} = K\, f(a')\, Re \sqrt{\frac{H}{b_0}} \qquad (2.6.17)$$

where the overall height H is substituted for the spill height H'. The constant K has to be determined experimentally. The function f(a') can probably be determined by numerical integration of equation (2.6.16).

The case of heat transfer through an opening in a vertical partition is studied in Appendix A.2. This case corresponds to an air curtain which is issued at zero air velocity. The formula obtained in the Appendix is

$$\frac{Nu}{Pr} = 0.044(Gr)^{0.59} \qquad (2.6.18)$$

3. EXPERIMENTAL

3.1 Experimental Setup.

An air curtain was installed between two well-insulated chambers, kept at constant temperatures.

The air curtain is shown schematically in Figure 1. It consisted of: a. outlet nozzle, b. return grille in the floor, c. ductwork, d. straighteners in the ductwork, and e. fans.

a. The outlet nozzle consisted of two sections, made of carefully rounded sheet metal on an iron frame. The cross section of each section was a curve, providing the air with a smooth and straight edged outlet. The nozzle thus formed was a long and narrow slot. The two sections could be moved one towards the other, so as to change the width of the outlet and to provide an air curtain of various thicknesses ($2\ b_0$). The width was varied between 0.115 ft. to 0.340 ft. Since the length of the slot was 53 inches, the aspect ratio was never smaller than 12 and the two-dimensional properties of the air jet were thus preserved.

The nozzle could be moved vertically to vary the height of the air curtain. The maximum height was $83\frac{1}{8}$ in. and provisions were made to reduce the height (H) by ten inches at a time.

b. The return grille in the floor was $53\frac{1}{2}$ in. long and $34\frac{1}{2}$ in. wide (in y-direction). During initial experiments it was found that the jet of air is inclined towards the warm side by a few degrees. By blocking eight inches of the return grille, at the cold side, better symmetry was obtained.

c. The ductwork connected the return grille to the nozzle. The rectangular ductwork contained the fans, the straighteners and a restriction gate in front of the fans. The restriction gate was used to vary the air velocity at the outlet.

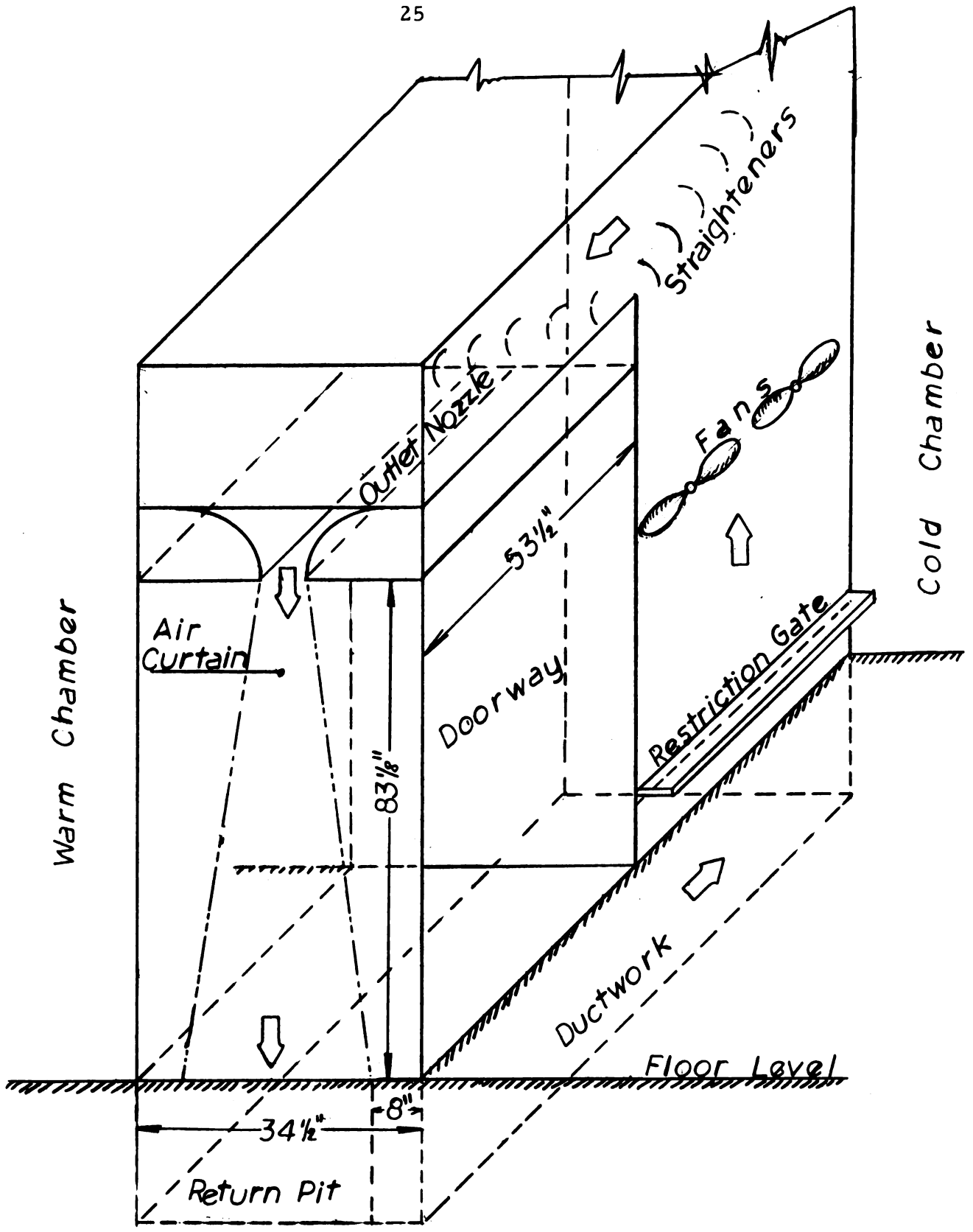

Figure 1. Schematic diagram of the air curtain used in this investigation.

d. Straighteners were placed in two locations in the ductwork, above the fans and above the nozzle. The straighteners consisted of about 16 pieces of sheet metal, rounded to form a quarter of a circle and held in place by plywood. The shape and location of the straighteners was varied until the air velocity along the outlet nozzle was uniform (in the z-direction) within ± 4.4% of the value at the center (z = 0).

e. Two fans were placed in parallel in the ductwork to provide the desired air velocity at the outlet. The fans used were type B No. 1185 by Aerovent, 18 in. in diameter, connected to a $\frac{1}{2}$ hp electric motor. The nominal air discharge from each fan, at pressure of $\frac{1}{8}$ in. water column, was 4,400 cfm.

The two chambers on the two sides of the air curtain were constructed of plywood and insulated with 3 in. of Microlite (by Johns-Manville) insulation material (density $\frac{3}{4}$ lb per cu. ft. k = 0.25 Btu per hr, ^{o}F, in.). The chamber on the left in Figure 1 was kept at high temperature with four electric heating mats, each providing 850 watts, connected in series with a thermostat. The chamber is 10 ft. high, 14 ft. long and 8 ft. deep (in the y-direction). The chamber on the right in Figure 1 was kept at lower and constant temperature by a one hp air-conditioning unit. This chamber is 10 ft. high, 14 ft. long, and 12 ft. deep (in the y-direction).

3.2 Instrumentation and Measurements.

The instruments used in this study are shown in Figures 2 and 3.

The probes for sensing velocity, turbulence and temperatures were placed on a traverse mechanism that could be moved vertically (x-direction) and across the jet (y-direction). The exact location of the probes in the y-direction was considered important and therefore a point gage was used, with the point removed and the probes placed on the end of the gage. The gage used was a Leroy, type A point gage, marked every 0.001 ft and accurate to ± 0.0001 ft.

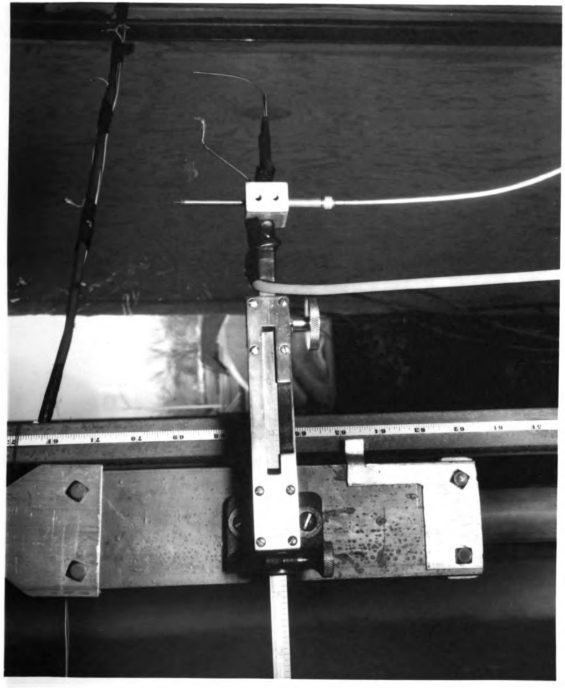

Figure 2. Traverse mechanism with probes.

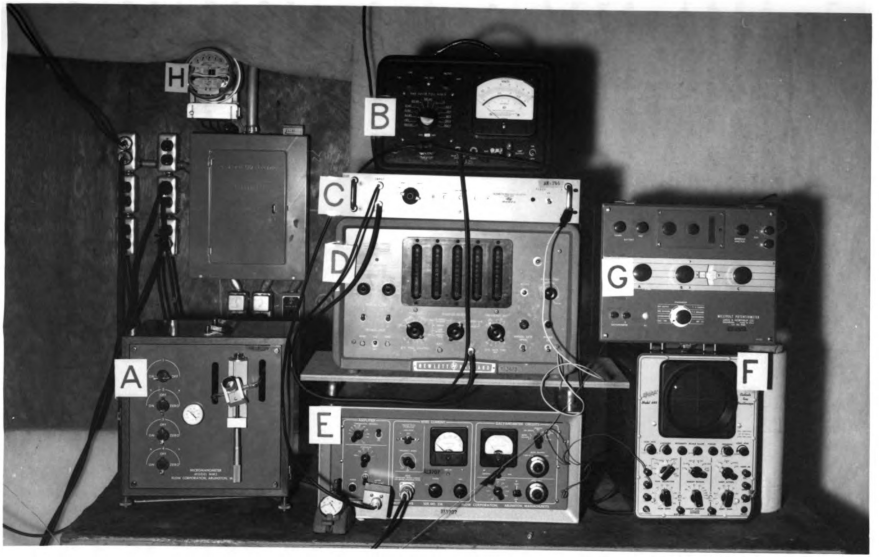

Figure 3. Instrumentation table.

3.2.a. Velocity.

The velocity was sensed by means of a No. 16 hypodermic needle as a total-head-impact-tube (on the right in Figure 2). The hypodermic needle tubing had an outside diameter of 0.065 in. and an inside diameter of 0.050 in. The end of the needle was carefully squared and burrs removed.

The pressure was sensed with a micro-manometer ("A" in Figure 3), model MM3 by Flow Corporation, which had butyl alochol as manometer fluid and nominal accuracy of ± 0.0002 in. of manometer fluid. Since this manometer had a slow response, only temporal mean values of total head could be measured.

The readings of the manometer were interpreted according to the equation

$$\Delta p = K_m \frac{\rho \bar{u}^2}{2} \qquad (3.1.1)$$

where

$$\Delta p = \gamma_m g d \qquad (3.1.2)$$

and K_m is a coefficient.

The coefficient K_m may vary somewhat from unity according to Research Publications of the ASME (1937), and should be determined experimentally. However, Goldstein (1938) reports that the value of K_m at speeds varying from 6 to 20 ft per sec did not differ from unity by more than ± 1 percent. Alexander (1953) calibrated a hypodermic needle of the same size and shape and found that K_m varied from 0.941 to 0.983, for the same velocity range. He further reports that impact tubes used in free jets are not subject to significant errors due to fluctuations in the angle of attack, up to an angle of 15 degrees.

In the present study most of the results are reported in the form of velocity ratios and therefore are not affected by small variations of the coefficient K_m.

Consequently in accordance with the common practice of other investigators, the impact measurements were not corrected for the effect of the angle of attack and the effect of the fluctuating components of velocity.

3.2.b. Temperature.

The temperature in the air stream was sensed by means of a copper-constantan (1938 calibration, 24 B&S gage) thermocouple located on the traverse mechanism (center in Figure 2). The EMF from the thermocouple was measured with a millivolt potentiometer ("G" in Figure 3; cat. No. 8686 by Leeds & Northrup; Philadelphia, Pa.). The millivolt measured were then converted to temperature by means of tables available with the instrument. The thermocouple was first calibrated with an accurate mercury in glass thermometer.

There might exist some difference between the temperature recorded by the thermocouple and the actual temperature of the air. This difference is due mainly to fluctuation in the air velocity. In addition, phase transformation, Joule effect and the like may affect the readings. A rough estimate by Hinze (1947) shows that the mean temperature recorded by the thermocouple is only a few percent too high at most. Since in this study the temperature profile was required, rather than sensible heat flux, the thermocouple and millivolt potentiometer measurements were considered satisfactory.

In addition the temperatures on the two sides of the air curtain were recorded hourly. For this purpose copper-constantan (1938 calibration, 24 B&S gage) thermocouples were placed 4 ft. from the centerline of the jet in the cold and warm sides at three distances x from the outlet nozzle (1 ft., 3 ft. and 5 ft.). The temperatures were recorded with a recording potentiometer (Brown Electronic Potentiometer, serial No. 712722, range 0-150^{o}F) equipped with an electrical clock.

The recorded temperatures were averaged over a test period and then the average temperatures at the three levels on each side, were averaged again to get a figure representing the temperature of the cold side (t_c) and the temperature of the warm side (t_w).

In addition, two thermocouples were located outside of the warm chamber to measure the outside temperature (t_0). These temperatures were also recorded hourly.

3.2.c. Heat.

The temperature of the warm side of the air curtain was kept constant by means of electric heating mats, placed on the floor and on the walls of the chamber. The temperature was constant within ± 2 degrees for any particular test period, but may have varied somewhat more between the various tests. The quantity of heat required to keep the warm chamber at constant temperature was measured by means of a watt-hour meter ("H" in Figure 3), placed in the circuit of the heating mats.

First the chamber was calibrated and the heat losses through the walls determined. This was done by blocking the opening with $\frac{1}{2}$ in. plywood and 3 in. insulation material, similar to that of the wall. The quantity of energy required to keep the warm chamber at constant temperature under these conditions was recorded for five days. This quantity of heat was regarded as loss through the walls (q_e in Btu per hr.) and was subtracted from the quantity of heat required to keep the warm chamber at constant temperature when an air curtain was applied over the opening.

Radiation heat transfer was neglected due to small temperature differences across the air curtain.

3.2.d. Turbulence.

A constant current hot wire anemometer ("E" in Figure 3; Model HWB ser. No. 216 by Flow Corporation, Arlington, Mass.), was used in the present investigation to determine the degree of turbulence. The hot wire probe (on the left hand side in Figure 2), was a standard 10 in. Flow Corporation probe. The filament was tungsten 0.0625 in. long and 0.00035 in. in diameter.

Figure 3 shows the various instruments used in conjunction with the hot-wire anemometer. The signal from the hot wire anemometer amplifier ("E"), was fed through a 7 KC low pass filter to a true-root-mean-square voltmeter ("B"; Model No. 320 by Ballantine Laboratories, Boonton, N. J.). The readings were very unstable, although the response time of the r.m.s. meter was increased to 2.5 seconds. In order to obtain an average of turbulence readings over a period of 100 seconds, the r.m.s. voltage was converted into frequency with the assistance of a voltage to frequency converter ("C"; Model 2210 by Dymec, Palo Alto, Calif.). The frequency was counted on an electronic counter ("D": Model 522B by Hewlett-Packard, Palo Alto, Calif.), with an open gate for the desired period.

The converter and counter were first calibrated by applying a steady voltage to the r.m.s. voltmeter and counting the frequency. The calibration curves are given in Figure 4.

After the probe had been connected to the hot wire anemometer the bridge was balanced cold, by using the bridge null variable resistor. The value of the bridge balance was recorded. Next the current was turned on and the bridge was balanced hot. The wire current "I" was measured by means of the galvanometer and the meter balance resistor. The value of the meter balance was recorded in units of four times the milliamperes. The square wave was then turned on and the compensation

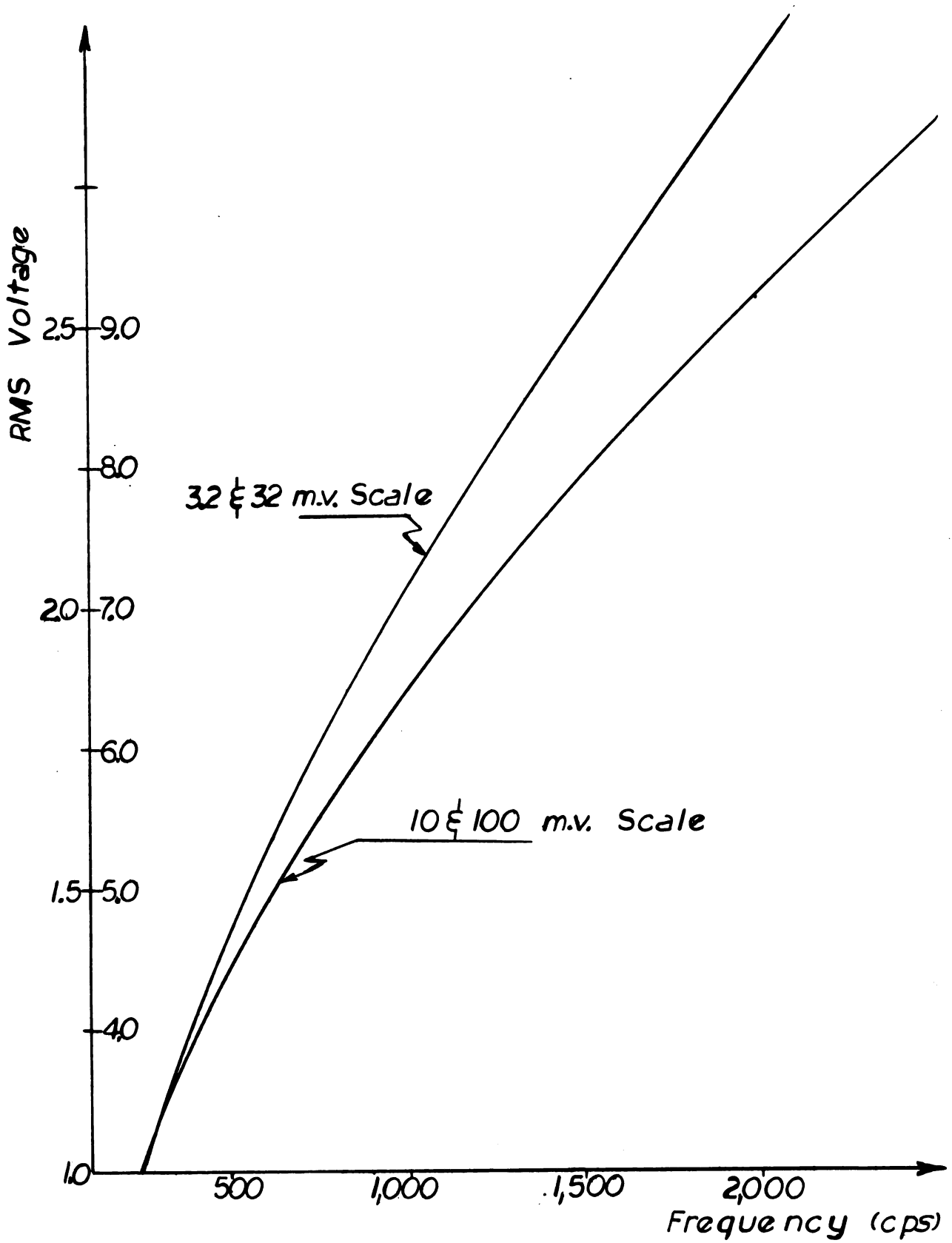

Figure 4. Calibration curves for the true root mean square voltmeter versus frequency count.

frequency adjusted until the oscilloscope pattern was a perfect square-wave. The square-wave and wire current were then switched off and the frequency counted on the electronic counter with an open gate for 100 sec. The r.m.s. value corresponding to this count was M_n, which is the noise level. The current was then turned on again and the frequency counted as before. The r.m.s. value corresponding to this count was M_{n+v}. The square wave was turned on again and the counting repeated. The r.m.s. value thus obtained was M_{n+v+s}. This procedure was repeated for every location of the hot wire probe. The resistance ratio was kept constant at 1.4 during all the tests.

3.3 Scope of tests and procedure.

The independent variables studied in this investigation were:

a. outlet velocity
b. outlet thickness
c. height

The heat transfer through the air curtain was determined for various values of the above variables.

Scope of tests. A total of 31 tests were run. They can be grouped in six series:

The first series of tests included the calibration of the warm chamber.

The second series included Tests 31 through 38. The height of the air curtain was $83\frac{1}{8}$ in. and the outlet thickness was 0.115 ft. In the third series (Tests 21 through 30) the height was kept constant at $83\frac{1}{8}$ in. but the outlet thickness was increased to 0.280 ft. The fourth series of tests included Tests 41 through 44. The height was $83\frac{1}{8}$ in. and the outlet thickness was increased to 0.340 ft.

Before the fifth series of tests (Tests 52 through 56) was run the height of the air curtain was changed to $73\frac{1}{8}$ in. This series included

three tests, for three different outlet velocities. The outlet thickness was fixed at 0.280 ft.

In the sixth series of tests the height of the air curtain was reduced to $63\frac{1}{8}$ in. The outlet velocity was varied between one test to another, but the outlet thickness was kept constant at 0.280 ft.

All tests with even numbers were conducted while a temperature gradient existed across the air curtain.

Procedure. For each test the velocity profiles were determined at the outlet and at three or more distances from the outlet. The velocity was measured every 0.05 ft. in the transverse (y -) direction, for small distances x from the outlet (x = 1 ft. and x = 2 ft.). For larger distances (x = 3 ft., 4 ft. and 5 ft.), the velocity was measured every 0.1 ft. in the y - direction.

For tests with temperature gradient across the jet the temperature profile was measured, at the same locations as velocity.

Both the velocity and temperature demonstrated large fluctuation in several locations. Therefore particular care was exercised to obtain a temporal mean value. In addition measurements were checked and back measurements taken, to ensure that stable conditions existed. The zero readings of all instruments were checked often and the instruments were recalibrated if necessary.

For one series of tests (Tests 42 through 46), the turbulence level was measured at the same locations as velocity.

After these measurements were completed the heat transferred through the air curtain was measured for the conditions of that particular test, for even number tests only. The quantity of heat required to keep the warm chamber at constant high temperature was measured for a period of about 12 hr. During this period the temperatures at the warm and cold chambers, and the outside temperature, were recorded hourly.

Five replica or more were made for each test and an average overall heat transfer coefficient was calculated.

For the last two series (Tests 50 through 66) only the outlet velocity and quantity of heat, together with the corresponding temperatures were measured. Neither temperature profiles nor velocity profiles in the air curtain were established for these tests.

Table 1. Summary of Tests

Test No.	Height H(ft)	Outlet width b_0(ft)	Aspect Ratio AR	Outlet Velocity $\bar{u}_0$(ft./sec.)	Re_0	$Re\sqrt{\frac{H}{b_0}}$ x 10^{-3}	h Btu / hr ft^2 ^{0}F	$\frac{Nu}{P_r}$ x 10^{-3}	Coefficients C_m	Coefficients C_T
22	6.92	.140	15.8	18.63	14,450	101.9	16.28	10.20	-	-
24	6.92	.140	15.8	15.52	12,596	88.6	14.08	9.00	.155	.200
26	6.92	.140	15.8	12.40	10,426	73.6	11.02	7.26	.170	.200
28	6.92	.140	15.8	21.76	17,869	125.9	18.82	12.30	.109	.200
30	6.92	.140	15.8	9.68	8,067	56.8	12.17	8.00	.220	.200
32	6.92	.0575	38.4	19.05	6,659	73.2	14.76	9.69	.109	.154
34	6.92	.0575	38.4	30.22	10,380	114.0	18.54	12.03	.109	.154
36	6.92	.0575	38.4	32.10	11,006	121.3	19.07	12.36	.109	.154
38	6.92	.0575	38.4	25.65	8,800	96.6	17.37	11.15	.109	.154
42	6.92	.170	13.4	13.57	13,488	86.3	11.91	7.67	.135	.220
44	6.92	.170	13.4	21.35	22,000	140.7	20.01	13.12	.121	.220
46	6.92	.170	13.4	16.56	16,600	106.1	17.14	11.05	.131	.220
52	6.10	.140	15.8	18.67	16,210	107.1	15.58	9.60	-	-
54	6.10	.140	15.8	13.78	11,950	79.0	11.94	6.95	-	-
56	6.10	.140	15.8	18.60	15,450	102.1	14.29	8.14	-	-
58	6.10	.140	15.8	22.18	18,650	123.1	19.25	11.91	-	-
62	5.26	.140	15.8	22.52	19,730	121.0	25.29	12.67	-	-
64	5.26	.140	15.8	16.28	13,710	84.3	16.69	8.30	-	-
66	5.26	.140	15.8	13.15	11,080	68.0	12.35	6.36	-	-

4. RESULTS AND DISCUSSION

The results of the tests are presented in Table 1 and in Appendix A.2.

4.1 Velocity.

The readings of the manometer which was connected to the total-head impact tube were interpreted according to the equation

$$\bar{u} = \sqrt{2 \gamma_m \frac{g}{\rho} d}$$

or

$$\bar{u} = 2.315 \sqrt{\frac{\gamma_m}{\rho}} \sqrt{d-d_0} \qquad (4.1.1)$$

where d is the manometer reading, in inches of manometer fluid, (n - Butyl Alcohol, F. W. 74.12), and d_0 is the manometer reading at zero velocity. The density of air and the density of the manometer fluid, at the proper temperatures, were taken from the International Critical Tables.

Most of the data are presented in a form of a ratio of the local velocity to the velocity at the outlet nozzle. This ratio is obtained from the formula

$$\frac{\bar{u}}{\bar{u}_0} = \sqrt{\frac{d-d_0}{(d-d_0)_0}} \qquad (4.1.2)$$

where no attempt is made to correct for temperature effect, because of small temperature differences.

In Figure 5 the data from the velocity measurements are compared with the probability distribution of momentum flux used to arrive at Reichardt's theory. For this comparison equation (2.2.1) was modified

as follows. By defining $b_{\frac{1}{2}}$ as the distance y at which the velocity is one half the value of the centerline, $\bar{u}_m$, it follows that

$$\exp\left(-\frac{b_{\frac{1}{2}}^2}{2\,C_m^2\,x^2}\right) = \frac{1}{2} \qquad (4.1.3)$$

from which

$$2\,C_m^2\,x^2 = \frac{b_{\frac{1}{2}}^2}{\ln 2} \qquad (4.1.4)$$

substitution of this expression in equation (2.2.1) yields

$$\frac{\bar{u}}{\bar{u}_m} = \exp\left(-\frac{y^2}{b_{\frac{1}{2}}^2}\ln 2\right) \qquad (4.1.5)$$

This function does not contain any arbitrary constants. Velocity from four tests, each at three distances from the outlet nozzle (x = 2 ft., 3 ft. and 5 ft.), for outlet width b_0 = 0.140 ft. and height H = 8$\frac{1}{8}$ in., are presented as data points in Figure 5. The solid line represents equation (4.1.5). This line is seen to correlate the data reasonably well. The standard deviation of the points was computed and found to be 0.0545 and the coefficient of variation was 0.133.

The velocity profiles as obtained from the tests are shown in Figures 5 through 10.

In Figure 6 the velocity profiles are shown for tests conducted with an air curtain having an outlet thickness of $2b_0$ = 0.115 ft. The aspect ratio for this series of tests was 38.4. The figure presents eight tests, with four different velocities. For each velocity there were two tests run, one test with temperature gradient across the jet (dotted line) and one test with no such temperature gradient (solid line).

The points given in the figure are data points obtained from measurements. The curves represent equation (2.2.5), with the constant C_m = 0.109. The correlation is seen to be quite satisfactory.

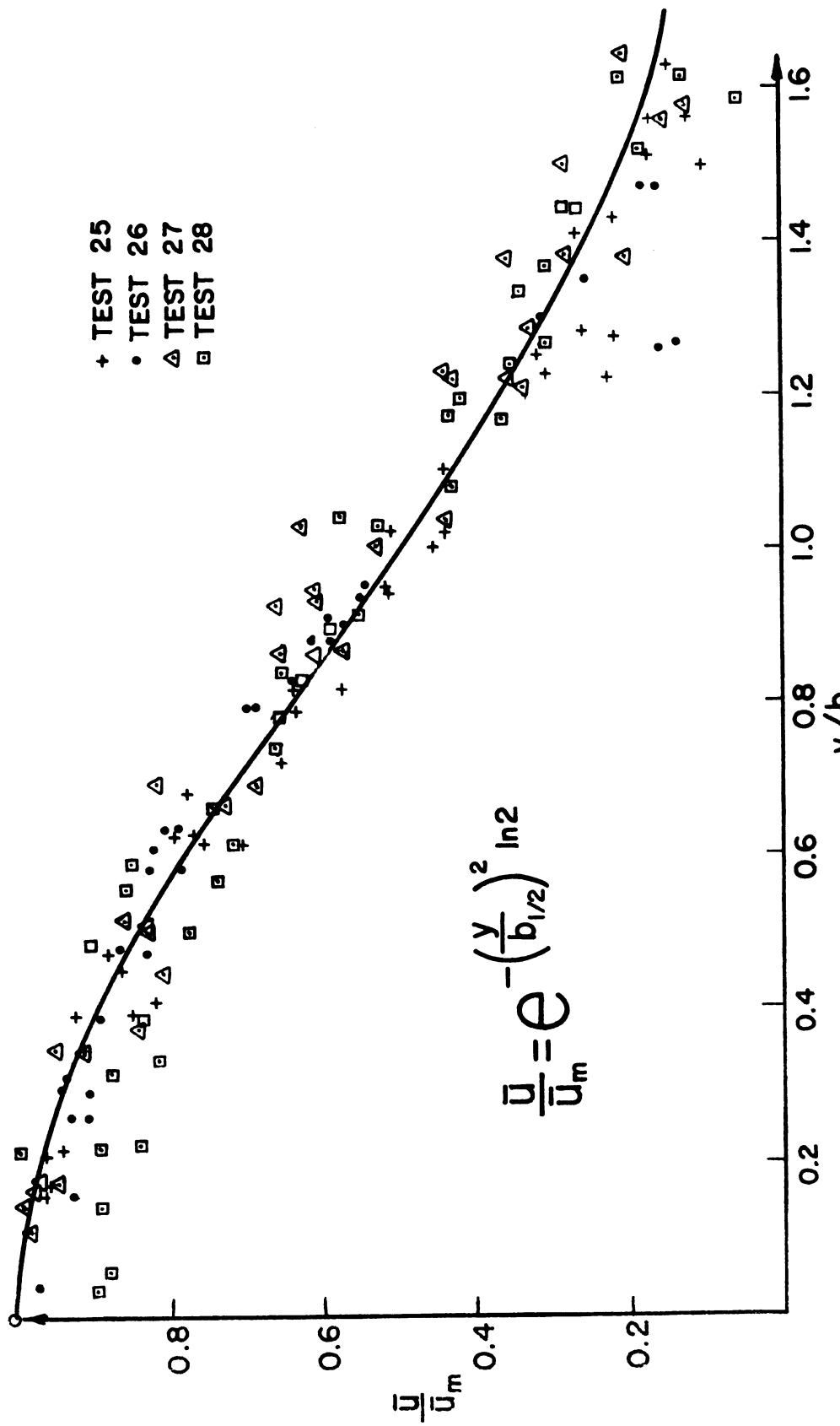

FIG. 5 VELOCITY PROFILE

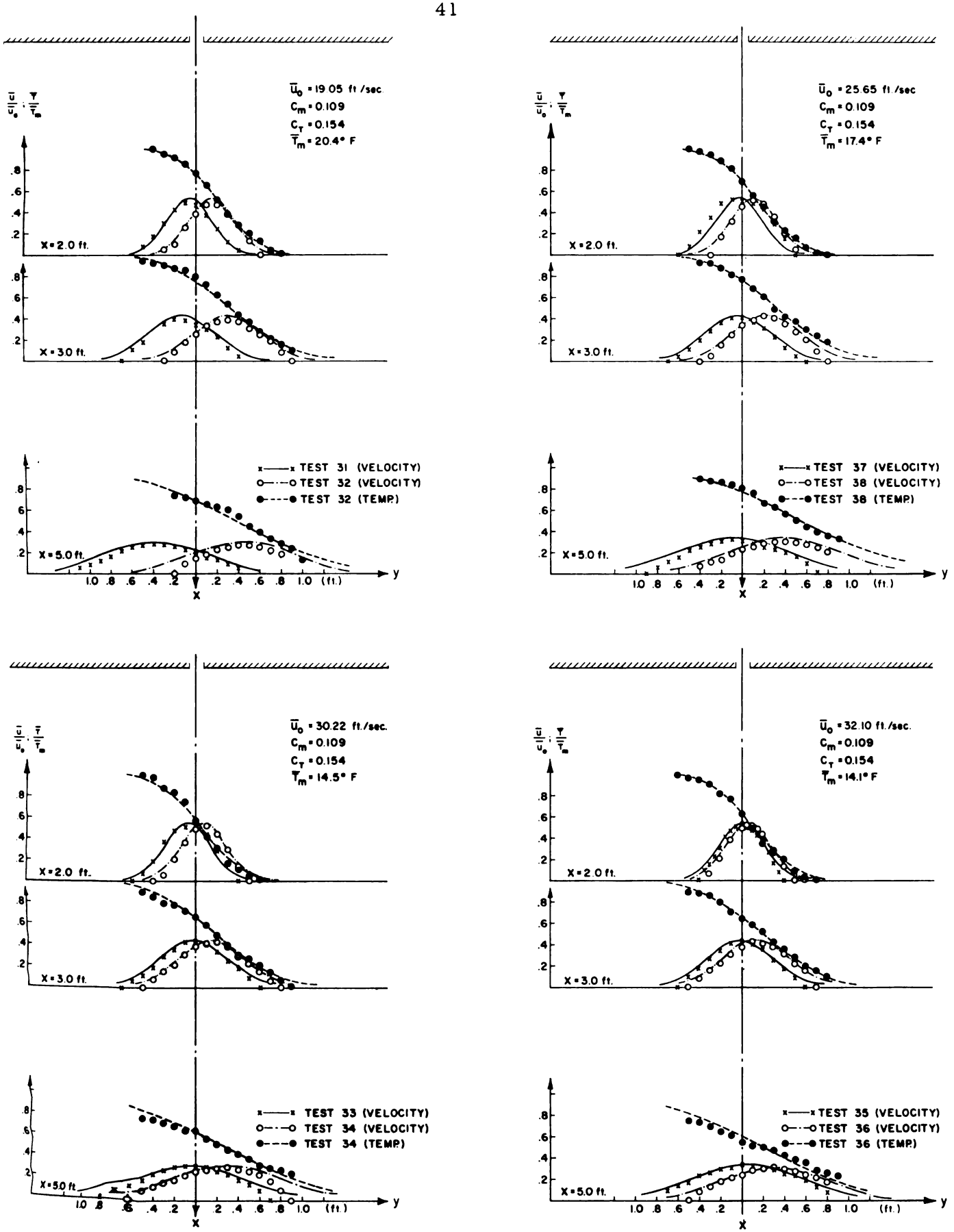

FIGURE 6. VELOCITY AND TEMPERATURE PROFILES.

$2b_o$ = 0.115 FT.

It should be noted that when no temperature gradient existed across the air curtain the jet was inclined a few degrees towards the left side (the warm side). When a temperature gradient did exist across the air curtain the jet was shifted towards the right side (cold side) and was inclined a few degrees to the right. The amount of shift from the original inclination to the left, depends mainly on the air velocity. The higher the velocity the less the jet is susceptible to shifting. The reason for such a shift was not well understood. At first it was believed that the air in the warm chamber expanded due to the heating and the larger pressure in the warm chamber caused the shift of the air curtain. However, in measurements made no static pressure difference could be detected across the jet. It was then thought that at higher temperature the constant C_m varies, causing an asymmetry in the velocity profile, resulting in deflection of the jet from its original location. However there was no indication in the literature to substantiate this explanation and it was abandoned. Turbulence measurements yielded some information that may be a clue to the explanation of the shift phenomena. This will be further discussed in section 4.2.

In Figure 7 the data from the next series of tests are presented. The outlet thickness of the jet was $2b_0 = 0.280$ ft., which gives an aspect ratio of 15.8.

The points given in the figure are data points and the curves represent equation (2.2.5), where the constant C_m was determined for each test separately. For high outlet velocity ($\bar{u}_0 = 21.76$ ft./sec.) the constant was $C_m = 0.109$. For the lowest velocity tested ($\bar{u}_0 = 9.68$ ft./sec.) the data was correlated well by equation (2.2.5) with $C_m = 0.220$.

The air curtain at 5 ft. from the outlet nozzle, in test 30 ($\bar{u}_0 = 9.68$ ft./sec.) when temperature gradient existed across it, is in a zone of transition. The effect of transverse pressure and buoyancy force is almost large enough to cause the curtain to break. It may be safely

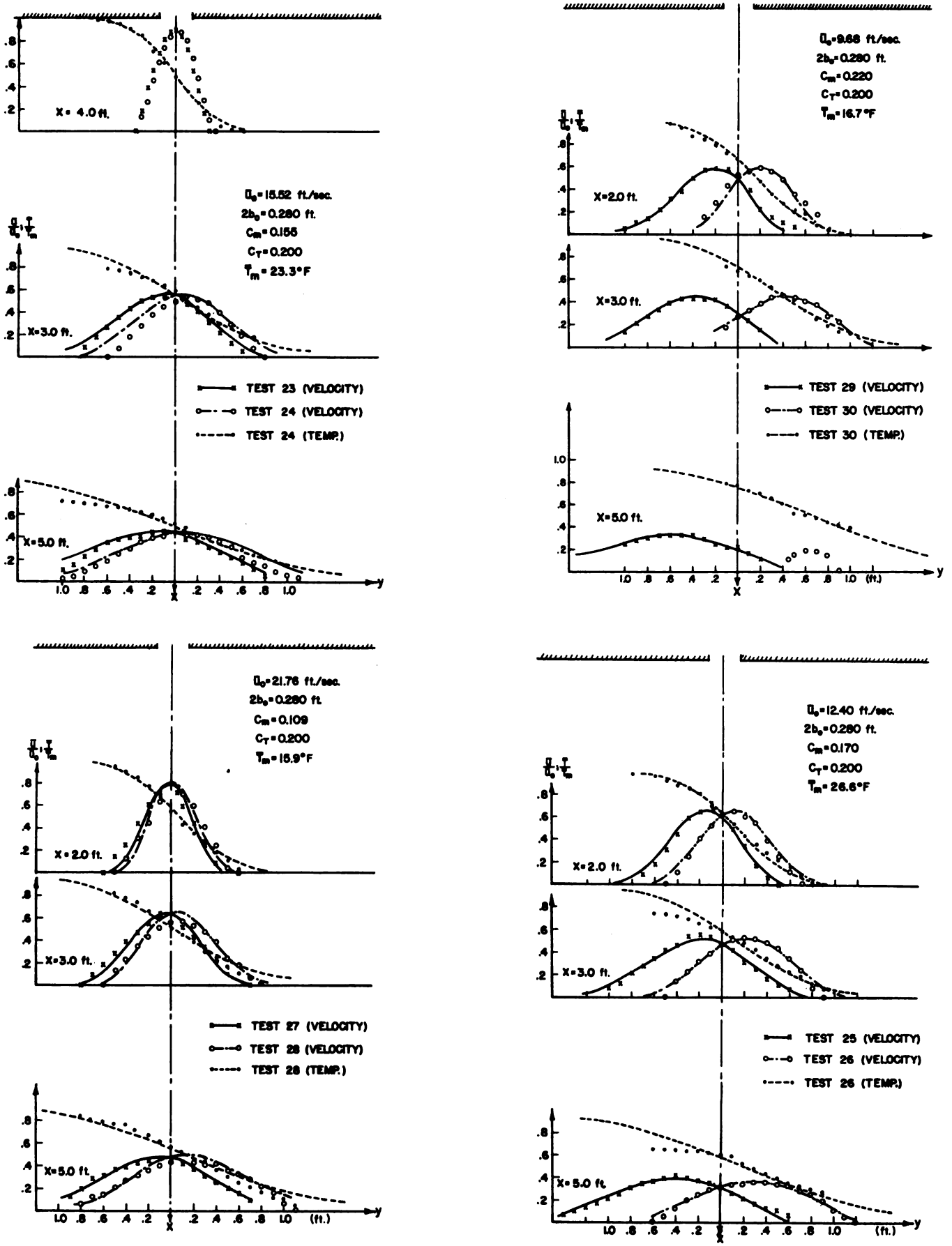

FIGURE 7. VELOCITY AND TEMPERATURE PROFILES.

$2b_o$ = 0.280 FT.

predicted that if the momentum of the air curtain at the outlet would be further reduced, the transverse forces will cause a transverse flow of air through the air curtain. In this case the air curtain actually ceases to exist and loses its effectiveness.

The phenomena of the shift of the air curtain from its original position, can be noticed in this series of tests also. Again the amount of shift depends on the outlet velocity and probably on the temperature difference across the air curtain. The higher the outlet velocity, the less the jet is shifted toward the cold side. The higher the temperature difference, the more the jet is shifted.

In Figures 8 through 10 velocity profiles are presented for an air curtain issued at a thickness of $2b_0 = 0.340$ ft. The aspect ratio in this case was 13.4. The points in the figures present data obtained from velocity measurement. The solid line represents equation (2.2.5). Again the constant C_m was found to vary from the theoretical value of 0.109, and was determined for each test separately. The tendency observed previously appears here too, namely, the lower the outlet velocity the larger the discrepancy between the theoretical $C_m (= .109)$ and the observed C_m.

In addition, to correlate the data from this series of tests by equation (2.2.5), it was necessary to divide the equation by the constant C_2. This constant varied with the outlet velocity. Thus the air curtain cannot be considered a truly two dimentional jet. The coefficient C_2 increased proportionally to the distance x from the outlet. Two feet from the outlet the coefficient was usually close to unity. At three feet it increased to 1.15, then to 1.19 at four feet and 1.21 at five feet from the outlet nozzle.

The shift of the jet due to the temperature difference is noticed in this set of experiments also. The amount of shift is found to be inversely proportional to the temperature difference across the air curtain.

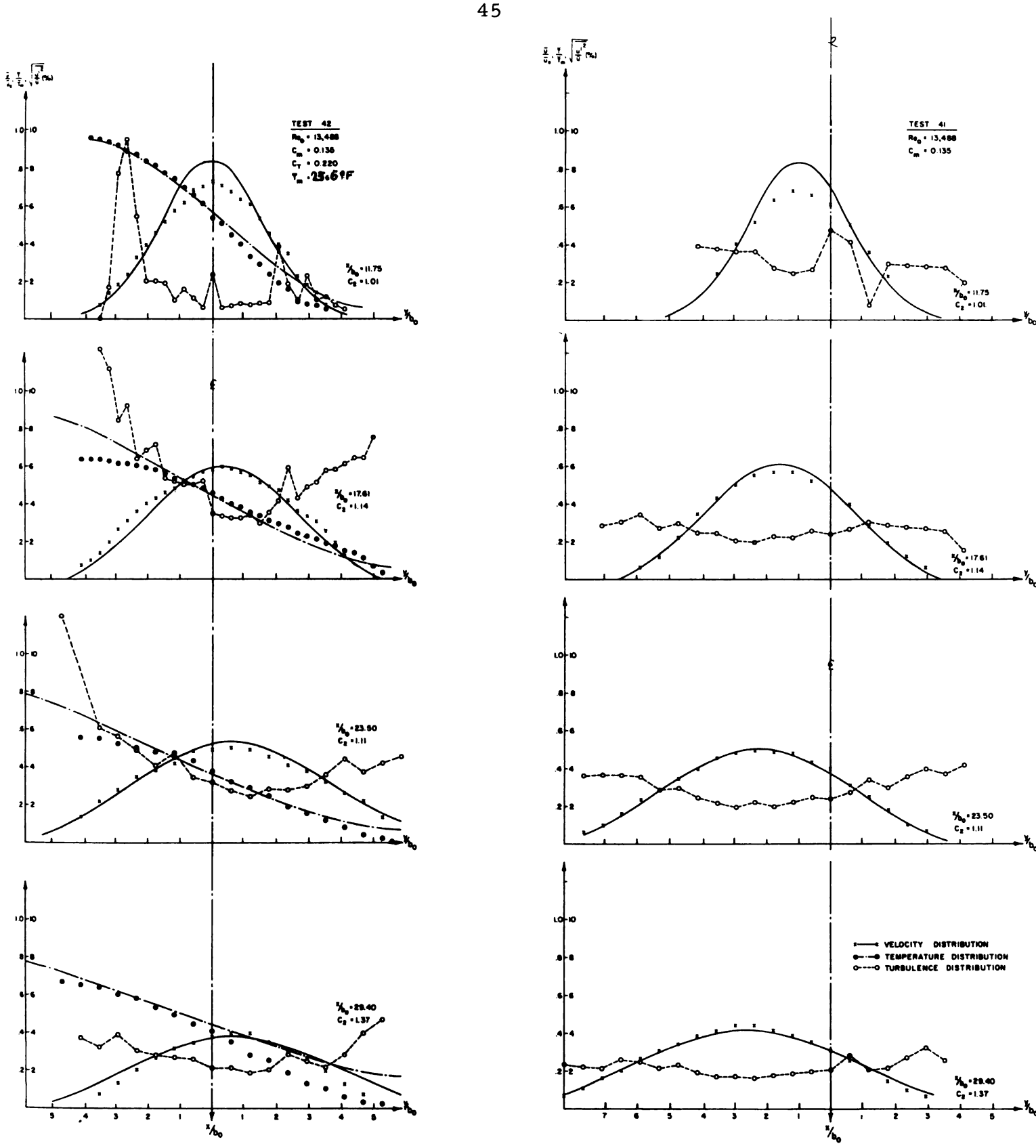

FIGURE 8. VELOCITY, TEMPERATURE AND TURBULENCE PROFILES. $2b_o = 0.340$ FT.

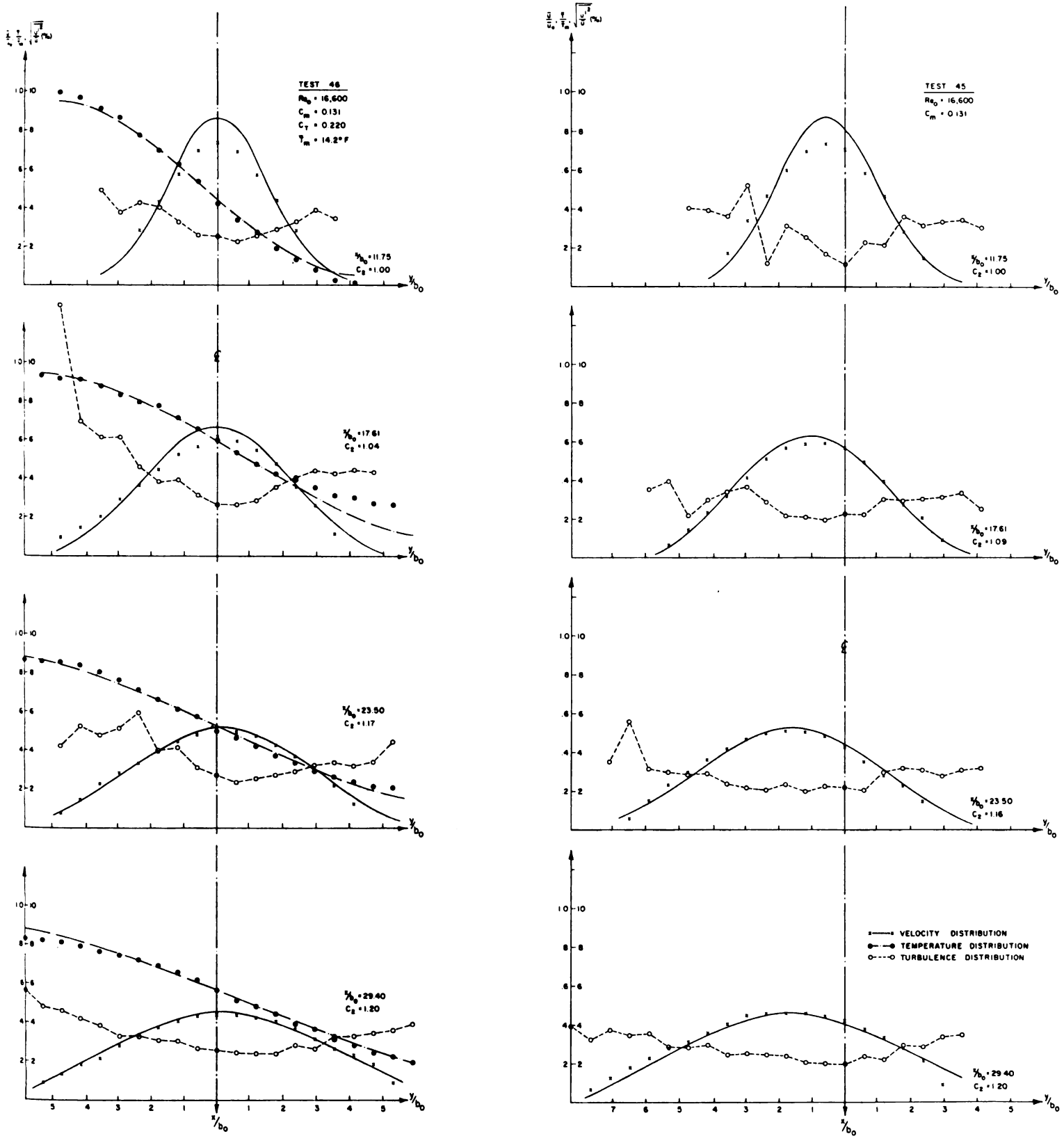

FIGURE 9. VELOCITY, TEMPERATURE AND TURBULENCE PROFILES. $2b_o$ = 0.340 FT.

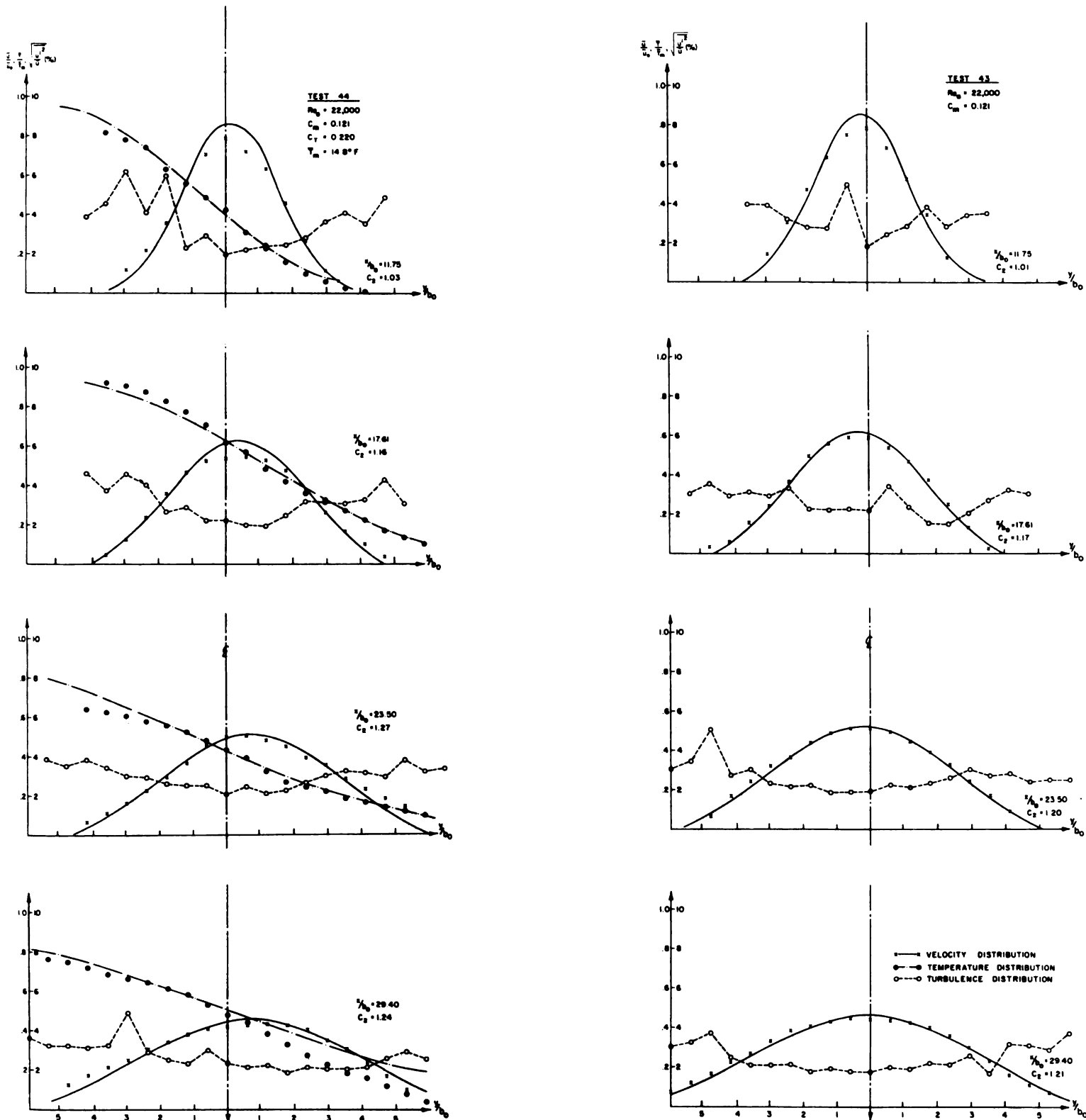

FIGURE 10. VELOCITY, TEMPERATURE AND TURBULENCE PROFILES. $2b_o$ = 0.340 FT.

In summation it may be said that equation (2.2.5) does correlate the data well and represents the velocity distribution in a two-dimensional air curtain. The constant C_m, as found in the literature (for a two-dimensional jet issued into an infinite medium), applies here only for high velocity and for high aspect ratios (Tests 31 through 38). For smaller aspect ratio and lower velocity the value of C_m does vary from 0.109. There were not enough data taken to determine the exact dependence of C_m and C_2 on either the aspect ratio or the outlet velocity. These two coefficients are probably temperature dependent. There is a considerable difference in velocity distribution of isothermal and heated jets both in the axial and transverse directions. This was pointed out by Cleeves (1947) and is substantiated here.

Some idea of the change of the coefficient C_m with the aspect ratio and outlet Reynolds number can be gained from the following Table and from Figure 11.

Table 2. The coefficient C_m for the various tests.

Test No.	Aspect ratio (AR)	u_0(ft/sec)	Re_0	$Re_0 x (AR) x 10^{-3}$	C_m
35-36	38.4	32.10	11,006	425	.109
33-34	38.4	30.22	10,380	398	.109
37-38	38.4	25.65	8,800	338	.109
31-32	38.4	19.05	6,659	256	.109
27-28	15.8	21.76	17,869	282	.109
23-24	15.8	15.52	12,596	199	.155
25-26	15.8	12.40	10,426	165	.170
29-30	15.8	9.68	8,067	128	.220
43-44	13.4	21.35	22,000	295	.121
45-46	13.4	16.56	16,600	222	.131
41-42	13.4	13.57	13,488	181	.135

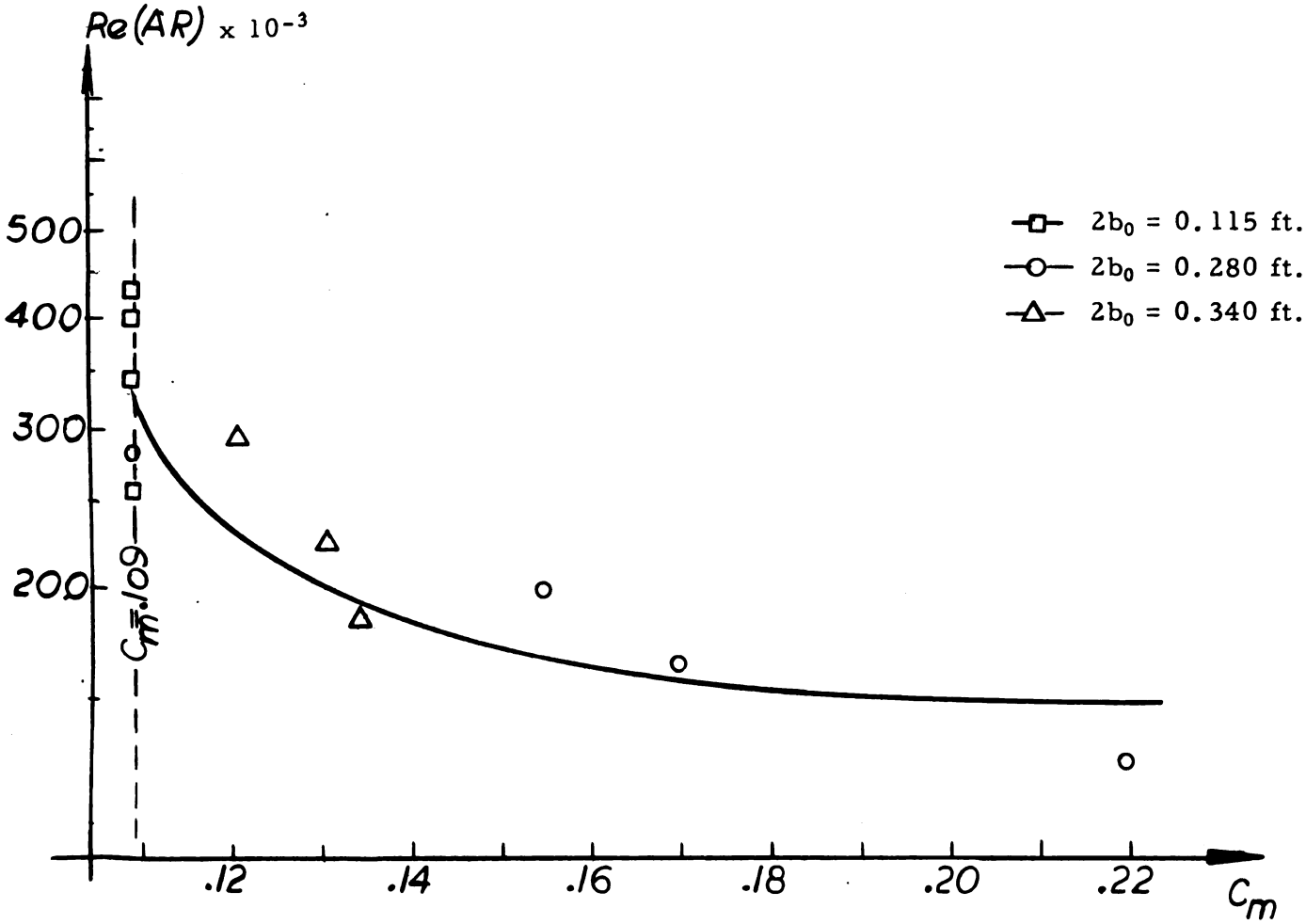

Figure 11. The coefficient C_m versus the product of the aspect ratio (AR) by the outlet Reynolds number (Re), on a semi-logarithmic paper.

It is quite obvious that C_m is inversely proportional to both the outlet Reynolds number and the aspect ratio. It is inversely proportional to the product of the Reynolds number by the aspect ratio.

From the data it appears that when this product is higher than 300,000, the jet can be considered as truly two-dimensional. When this product decreases, the discrepancy between the air curtain and a true two-dimensional jet increases.

In Figure 12 the theoretical stream function was plotted. For this purpose equation (2.2.11) was made dimensionless as follows:

$$\frac{\Psi}{\bar{u}_0 b_0} = \sqrt{\sqrt{\pi} C_m} \sqrt{\frac{x}{b_0}} \operatorname{erf}(\eta) \qquad (4.1.6)$$

A theoretical value for the coefficient was used in the plot, namely, $C_m = 0.109$.

The lines in Figure 12 represent the stream function at equally spaced values. The figure is given only up to a distance x = 5 ft. from the outlet nozzle. The function was not extended to the zone where the spill occurs since the spill mechanism is not well understood and the stream function from the previous equation most certainly does not apply to this region. However the figure demonstrates the entrainment and it is quite obvious that $\bar{u}_m \propto x^{-\frac{1}{2}}$ and $Q \propto x^{+\frac{1}{2}}$.

4.2 Turbulence.

The theoretical shear stress is plotted in Figure 13 in a dimensionless form, using equation (2.3.7), namely

$$\sqrt{\frac{\tau}{\rho \bar{u}_0^2}} = \left[\frac{1}{\sqrt{2}\, x/b_0} \exp(-\eta^2) \operatorname{erf}(\eta) \right]^{\frac{1}{2}} \qquad (4.2.1)$$

where

$$\eta = \frac{y}{\sqrt{2} C_m x} = \frac{y/b_0}{\sqrt{2} C_m x/b_0} \qquad (4.2.2)$$

From the figure it is quite apparent that the shear stress has two maxima, and is symmetrical around the centerline. This plot represents a semi-theoretical distribution, since it is based on Reichardt's theory, which correlates experimental data adequately. The plot is theoretical in that it is based on calculated values rather than experimental measurements.

In Figure 14 the coefficient of apparent viscosity ϵ_m is plotted in a dimensionless form, according to equation (2.3.11),

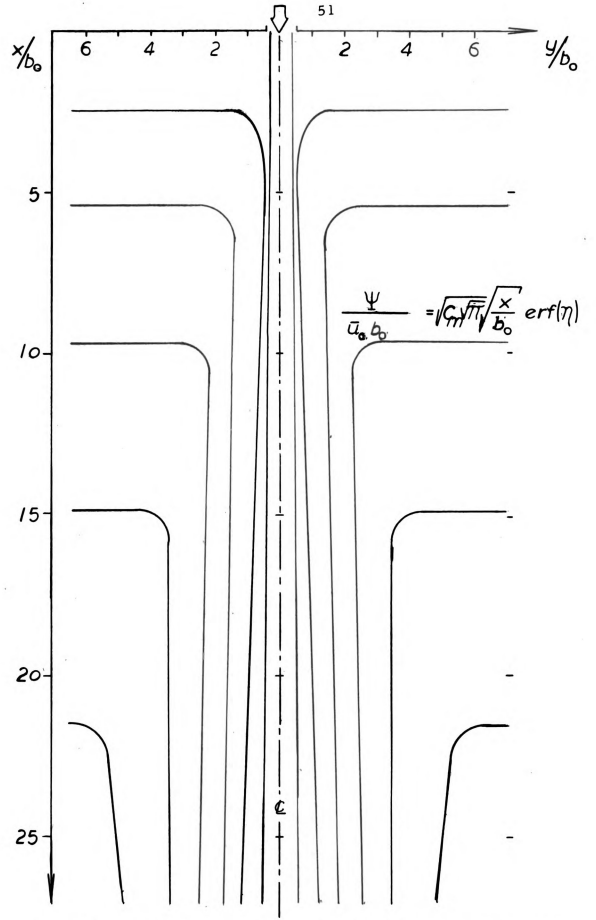

Figure 12. Semi-theoretical stream function in a dimensionless form ($C_m = 0.109$).

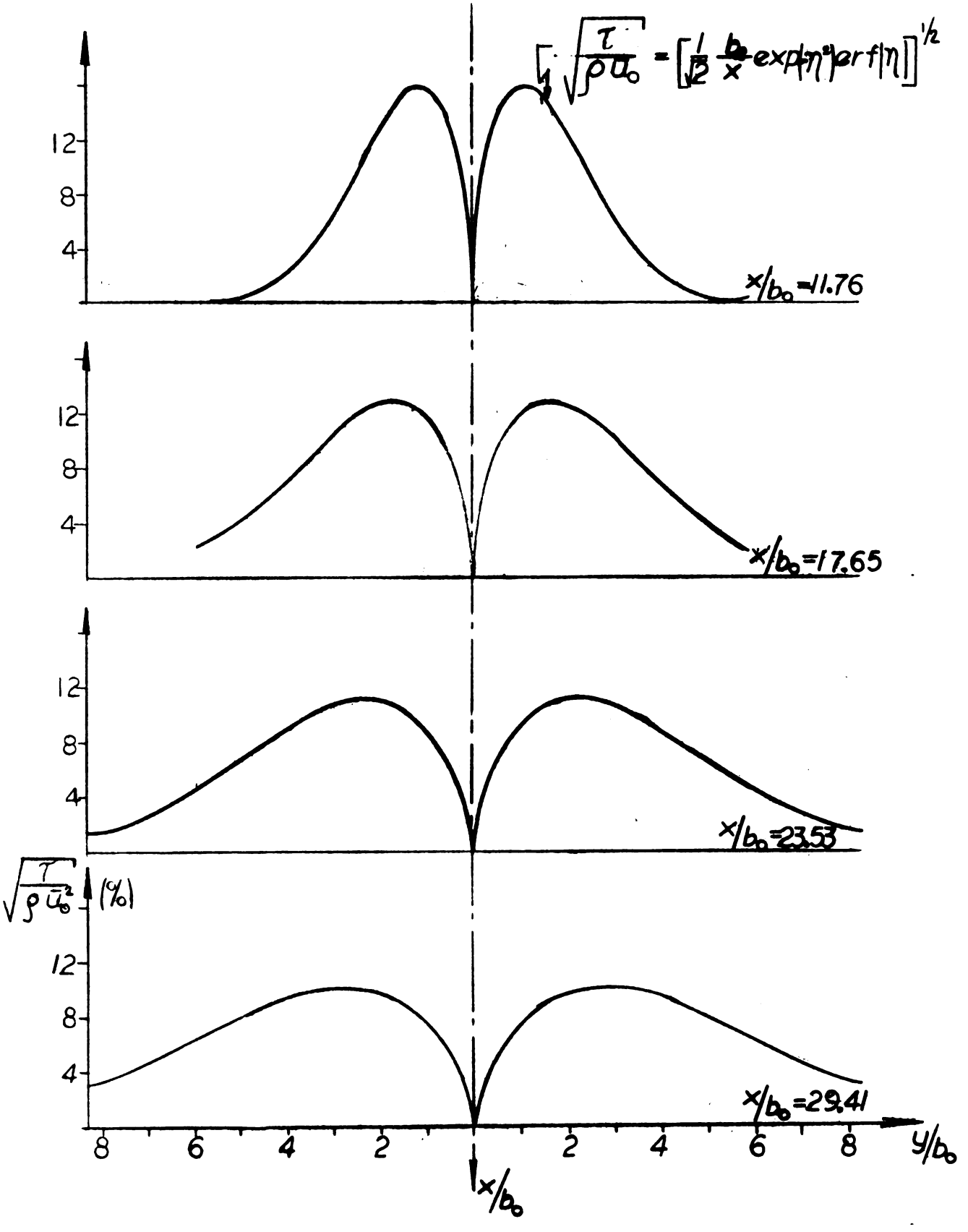

Figure 13. Semi-theoretical shear distribution, related to the outlet velocity, at various locations in the flow (C_m = 0.109; b_0 = 0.170 ft.).

$$\frac{\epsilon_m}{\nu} = Re_0 \sqrt{\frac{C_m^3 \sqrt{\pi}\, x}{8 b_0}}\ \frac{erf(\eta)}{\eta} \qquad (4.2.3)$$

where

$$\eta = \frac{y}{\sqrt{2}\, C_m x} \qquad (4.2.4)$$

The plot was made for four distances x/b_0 with $C_m = .109$ and for a Reynolds number at the outlet corresponding to that of Test 44, namely

$$Re_0 = 22,000$$

Figure 14 can be considered as a semi-theoretical plot, based on the exponential velocity profile. This figure may be used for determining the heat transfer coefficient, if Reynolds' analogy or some other relationships are assumed. It should be noted that the ratio ϵ_m/ν reaches a maximum value at the centerline of the jet and has a general shape similar to that of the velocity distribution. The assumption that $\epsilon_m >> \nu$ is further confirmed for the particular values chosen here.

Another form of the shear stress distribution is shown in Figure 15. The shear stress τ is now related to the local velocity $\bar{u}$, rather than to the outlet velocity $\bar{u}_0$ that was used in Figure 13. For this purpose equation (2.3.7) was modified as follows

$$\sqrt{\frac{\tau}{\rho\, \bar{u}^2}} = \left[\sqrt{\frac{\pi}{2}}\ \frac{C_m}{2} \exp(\eta^2)\, erf(\eta) \right]^{\frac{1}{2}} \qquad (4.2.5)$$

where

$$C_m = 0.109 \qquad (4.2.6)$$

It should be noted that curves obtained have quite a different shape than those in Figure 13. The curves have one minimum at the centerline of the jet and increase without bound toward the two edges.

Since the shear stress is given by

$$\tau = -\rho\, \overline{u'v'} \qquad (4.2.7)$$

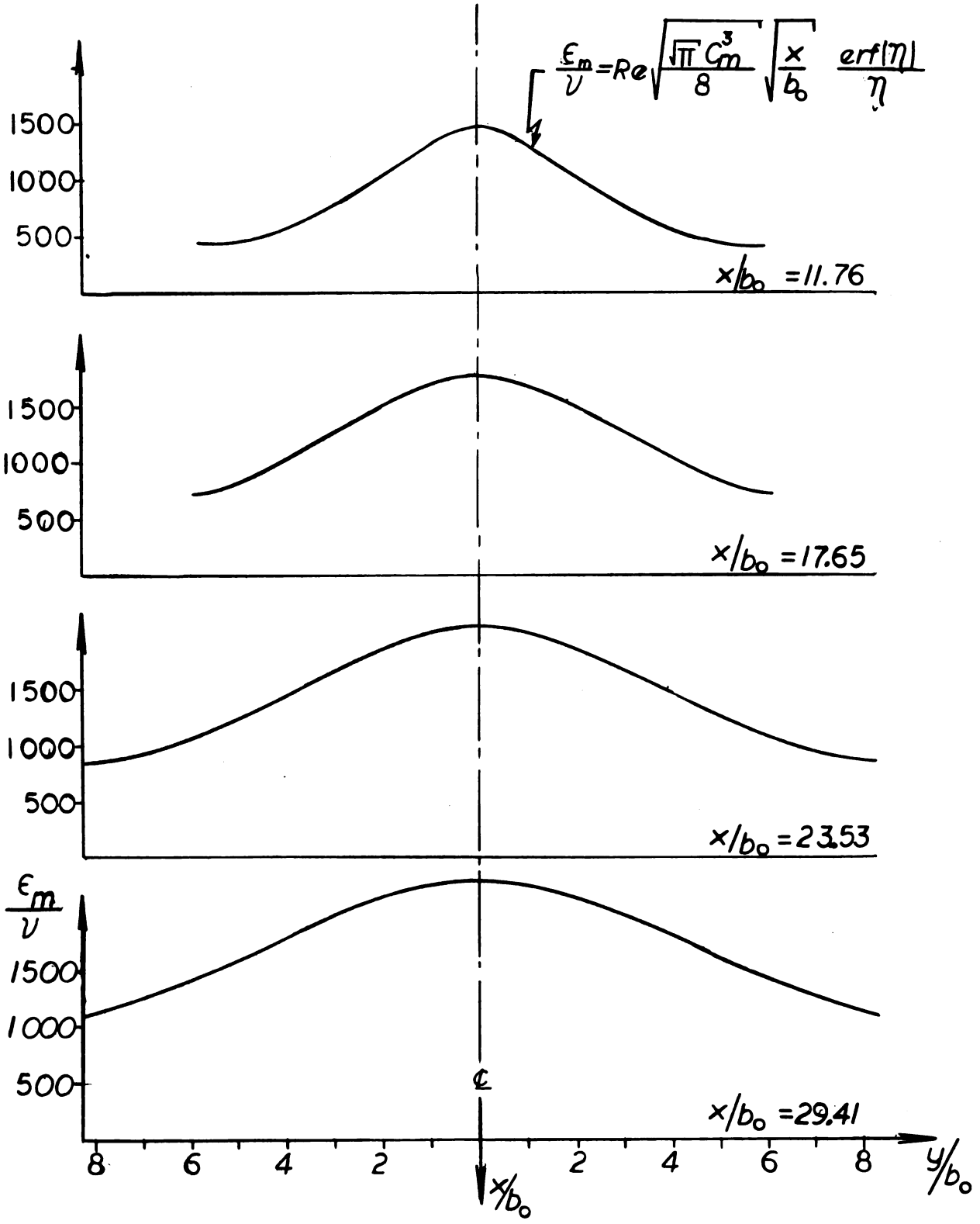

Figure 14. The ratio of apparent viscosity to the kinematic viscosity at various locations in the flow (Re = 22,000; C_m = 0.109 and

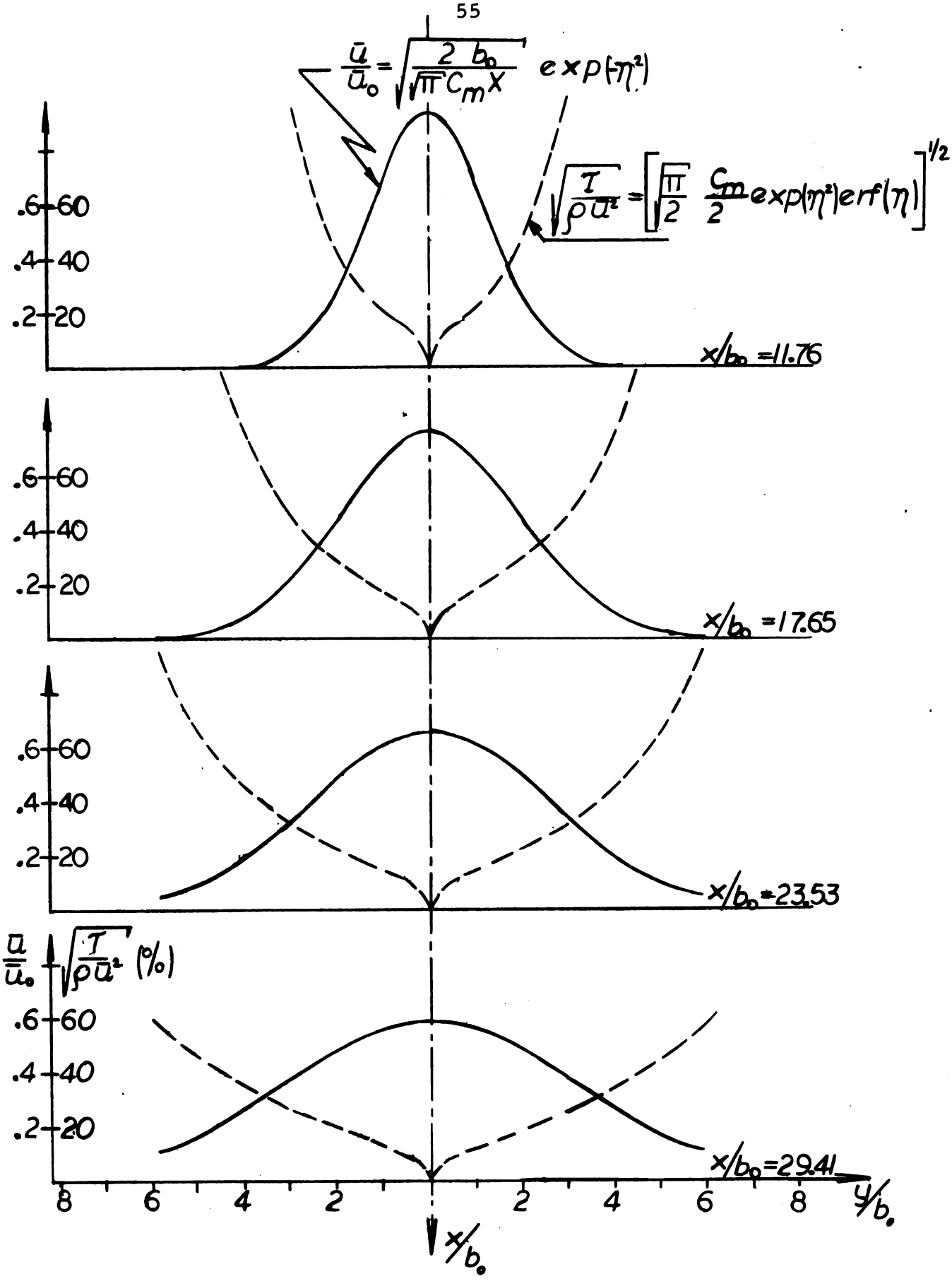

Figure 15. Semi-theoretical shear distribution, related to the local velocity (dotted line) and the velocity distribution (solid line), (C_m = 0.109, b_o = 0.170 ft.).

and since it was assumed that u' is proportional to v', it may be concluded that Figure 15 represents the turbulence, when a different scale is used in the ordinate. The assumption that v' is proportional to u' and that $\overline{u'v'}$ is proportional to u' is quite a drastic one, and was neither investigated nor confirmed in this investigation. However, as pointed out in section 2.3, it is frequently used and it gives some insight into the turbulence process, even though it may not be quantitatively exact. With this in mind Figure 15 may be compared with Figures 8 through 10. In these figures the results from turbulence measurements are plotted in a dimensionless form, together with velocity profiles. All data were taken with an air curtain issued at a thickness of $2b_0 = 0.340$ ft. The outlet velocity was varied from 13.57 to 21.35 ft. per sec.

In Figure 8 data are plotted for an air curtain issued at 13.57 ft. per sec. (Tests 41 and 42). There are eight turbulence profiles representing four distances from the outlet nozzle. On the right hand side in Figure 8 are the velocity and percent turbulence profile when there was no temperature gradient across the jet. On the left hand side are velocity, percent turbulence and temperature profiles when such a gradient did exist. The dotted line connects data points from turbulence measurements, conducted with the hot wire anemometer. The points represent percent turbulence or $(\sqrt{\overline{u'^2}}/\bar{u}) \times 100$. The percent turbulence at the outlet was less than one percent in most cases. At a distance 2 ft. from the outlet the percent turbulence was very high when a temperature gradient existed across the air curtain. This may be due to the fact that at a distance 2 ft. from the nozzle the jet is still in the zone of transition where the flow is unstable and percent turbulence may be high. Further from the outlet nozzle, where the flow becomes fully developed, the percent turbulence decreases, and keeps decreasing with x.

For the air curtain with no temperature gradient the turbulence is approximately symmetrical around the centerline. There is always a

minimum at the center point, and a gradual increase of percent turbulence progressing away from the centerline. It should be noted that the very high percent turbulence at the edges of the jet is due to a low velocity at these points, rather than high fluctuations of the velocity.

The air curtain with a temperature gradient across it presents quite a different situation. Here the turbulence profile is asymmetric, where the turbulence on the warm side has, in most cases, a peak much higher than at a corresponding point on the cold side. For example at a distance of 3 ft. from the outlet nozzle the turbulence on the warm side is about 12.4 percent at a distance y = 0.60 ft. from the centerline, compared to 5.8 percent at corresponding y-location on the cold side.

In Figure 9 data from Tests 45 and 46 are presented. The outlet velocity is 16.56 ft. per sec. and the percent turbulence at the outlet is always less than 0.82 percent. The tendencies observed previously are present also in this figure, i.e., the higher percent turbulence on the warm side and the gradual decrease of turbulence progressing away from the outlet nozzle. The peaks at the warm side, however, are not as pronounced as in the Figure 8. This may be due to a smaller temperature difference across the jet (14.2^{o}F compared with 25.6^{o}F in previous test) or it may be due to the higher outlet velocity.

In Figure 10 the data from tests 43 and 44 are presented. The outlet velocity is 21.35 ft. per sec. and the percent turbulence at the outlet is always less than 0.65 percent. The observation that the peak in the turbulence profile is higher in the warm side than in the cold side, is certainly noticeable here too. Also, the percent turbulence decreases as the jet progresses away from the outlet nozzle.

In summation, it may be said that the percent turbulence decreases as the air curtain progresses away from the outlet nozzle. In addition, there exists an asymmetry in the turbulence profile. For a jet issued at uniform temperature into a medium at the same temperature the

turbulence profile is symmetrical around the centerline. However, for a jet having a temperature gradient across it, the turbulence at the warm side is considerably higher than the turbulence on the cold side. This asymmetry is proportional to the temperature difference across the jet, and may also be inversely proportional to the velocity at the outlet. The exact effect of temperature and outlet Reynolds number were not determined in the present investigation. The higher turbulence on the warmer side causes several phenomena. Since the turbulence is higher it may be safely assumed that the shear stress is higher on the warm side. This causes an asymmetry in the forces acting on the jet, which in turn causes the jet to be deflected from its original position. The phenomenon of the jet deflection toward the cold side, due to the temperature gradient, was observed and discussed before. This deflection is caused by the higher percent turbulence, even though the exact mechanism cannot be stated explicitly. It may be stated that the higher turbulence on the warm side is due to increase of the apparent viscosity ϵ_m proportionally to the temperature, which is similar to the effect of temperature on the kinematic viscosity. However, the coefficient ϵ_m represents a physical process which is not well understood and the above statement does not help in clarifying the phenomenon and its causes.

It can be safely assumed that the turbulence is increased due to an increase in the buoyancy forces. This assumption is somewhat substantiated by the fact that the degree of asymmetry is proportional to the temperature difference across the jet. The higher temperatures on the warm side cause warm air to rise at the edge of the jet. This process of counterflow induces turbulence at the edge of the jet, which then progresses into the main flow.

The effect of temperature on the apparent viscosity and the percent turbulence in a free-turbulent shear flow deserves further attention and study.

4.3 Temperature.

The temperature profiles, as obtained from measurements, are presented in Figures 6 through 10. The temperatures are presented in a dimensionless ratio $\overline{T}/\overline{T}_m$ where $\overline{T} = t - t_c$ and $\overline{T}_m = t_w - t_c$. The temperatures of the cold and the warm sides were established at a distance of 2 ft. from the outlet nozzle. The traverse mechanism with the thermocouple was moved towards the warm side until the temperature reached an asymptotic value. The same procedure was followed in the cold side. Since at distances larger than x = 2 ft., the traverse mechanism could not be moved far enough to reach an asymptot, the temperature difference at x = 2 ft. was considered the maximum temperature difference $\overline{T}_m$.

In Figure 16 the data from temperature measurements are compared with the form of the error function which was assumed for the temperature distribution. For this comparison equation (2.5.4) was modified as follows. By defining $b_{\frac{1}{4}}$ as the distance y_T at which the temperature is three quarters (or one quarter) of the maximum temperature difference existing across the air curtain, $\overline{T}_m$, or

$$\text{at} \quad y = \pm b_{\frac{3}{4}}, \quad \overline{T} = \tfrac{1}{4}\,\overline{T}_m \text{ and } \overline{T} = \tfrac{3}{4}\,\overline{T}_m \tag{4.3.1}$$

it follows that

$$\frac{\overline{T}}{\overline{T}_m} = \tfrac{3}{4} = \tfrac{1}{2}\left[1 + \operatorname{erf}\left(\frac{b_{\frac{1}{4}}}{\sqrt{2}\,C_T x}\right)\right] \tag{4.3.2}$$

or

$$\operatorname{erf}\left(\frac{b_{\frac{3}{4}}}{\sqrt{2}\,C_T x}\right) = \tfrac{1}{2}$$

therefore

$$\frac{b_{\frac{3}{4}}}{\sqrt{2}\,C_T x} = 0.480$$

or

$$\sqrt{2}\,C_T x = \frac{b_{\frac{3}{4}}}{0.480} \tag{4.3.3}$$

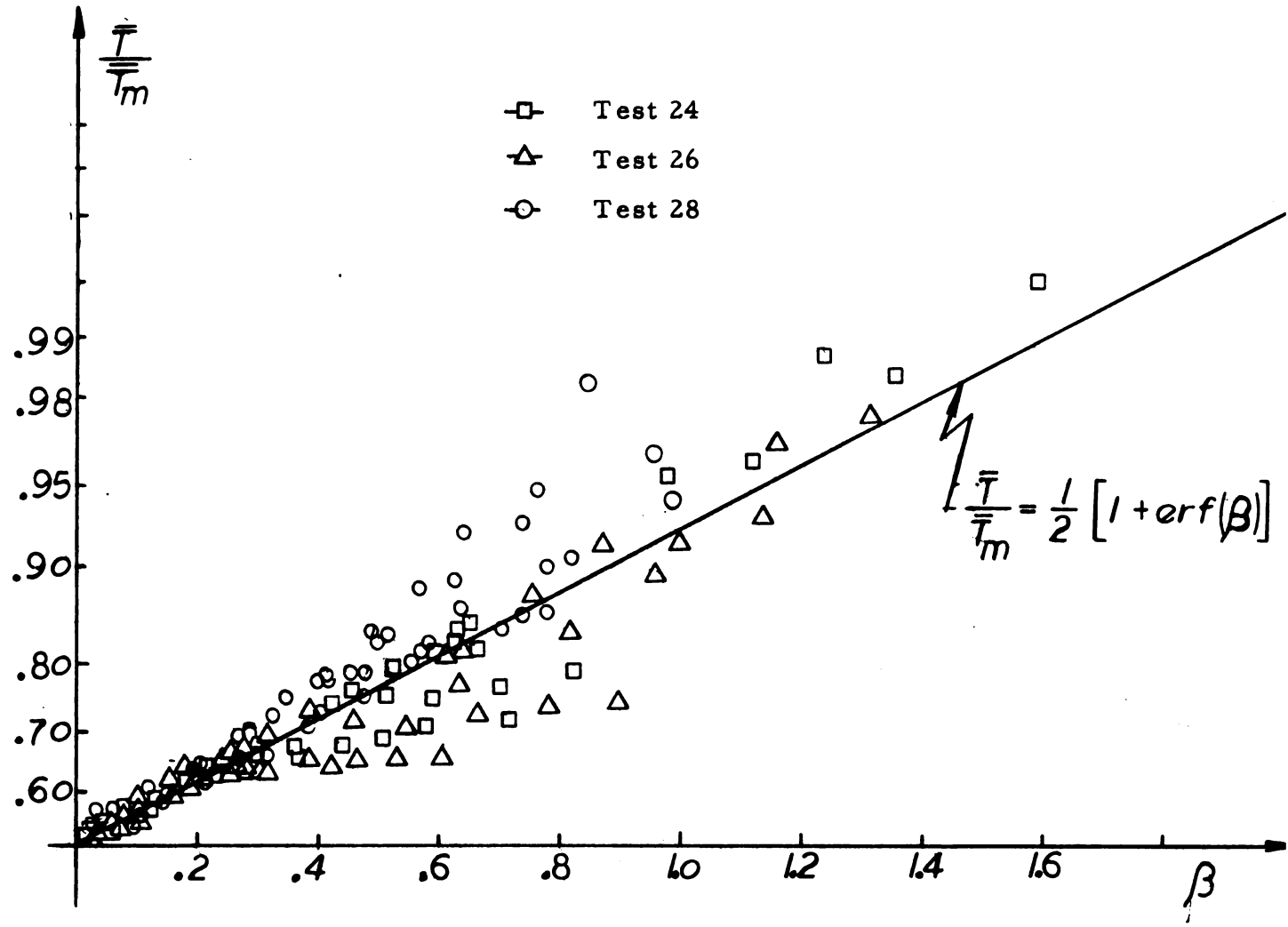

Figure 16. Dimensionless temperature profile plotted on an arithmetic probability paper.

Substitute equation (4.3.3) into equation (4.3.2) to get:

$$\frac{\bar{T}}{\bar{T}_m} = \frac{1}{2}\left[1 + \text{erf}\left(\frac{0.480\ y}{b_{\frac{3}{4}}}\right)\right] \qquad (4.3.4)$$

This function does not contain any arbitrary constants.

Temperature ratios from three tests, each at three distances from the outlet nozzle (x = 2 ft., 3 ft. and 5 ft.), for outlet thickness of $2b_0 = 0.280$ ft. and height h = $83\frac{1}{8}$ in. are presented as points in Figure 16. The solid line

represents equation (4.3.4). Since the figure is drawn on an arithmetic probability paper, this is a straight line. Equation (4.3.4) is seen to correlate the data reasonably well. Close to the center (at $y_T = 0$; $\frac{\overline{T}}{T_m} = \frac{1}{2}$) the correlation is excellent, since the curve was made to fit the data, at this region - or $y_T = 0$ was defined at the point where $\frac{\overline{T}}{T_m} = \frac{1}{2}$. Further away from the center the correlation is less satisfactory. This is due to the fact that small errors in measurement, due to turbulence and inaccuracies, are multiplied as one progresses away from the centerline.

The solid line in Figure 16 was also used as a mean to determine the theoretical β and then the theoretical C_T. From the temperature measurements in each location the dimensionless temperature T/T_m was formed. The value of β was then obtained from the abcissa in Figure 16, corresponding to the ordinate T/T_m. Since the value of x, as well as the value y_T were known, a theoretical value of C_T was then calculated from the formula

$$C_T = \frac{y_T}{\sqrt{2} \times \beta} \qquad (4.3.5)$$

The values of the coefficient C_T thus obtained are presented in Figures 17 through 19.

In Figure 17 the variation of the coefficient C_T with respect to y_T is shown, for the different velocities and distances x from the outlet. This figure presents the results of tests 32 through 38, where the thickness of the air curtain at the outlet was 0.115 ft. and the aspect ratio was 38.4. The scatter of the data is not too wide and may be due to experimental errors and effects of turbulence. An average value of $C_T = .154$ is suggested as representing the data of this series of tests.

It should be noted that for the same series of tests $C_m = .109$ was confirmed. Therefore, for a two-dimensional jet issued into an infinite medium a value of

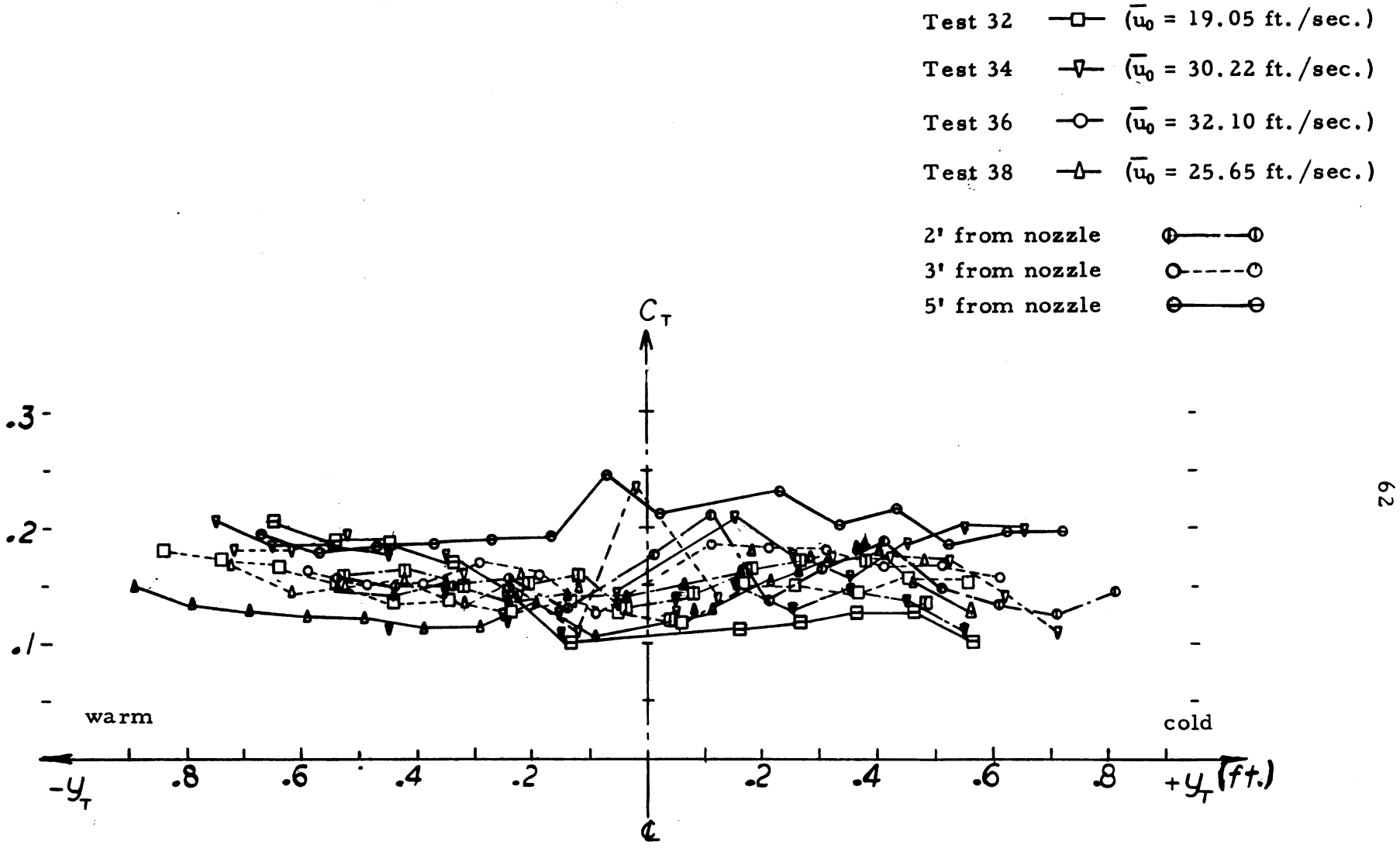

Figure 17. Plot of the coefficient C_T versus the distance y_T ($2b_0$ = 0.115 ft.).

$$C_T = 0.154 \tag{4.3.6}$$

or

$$\delta = \frac{C_T}{C_m} = \sqrt{2} \tag{4.3.7}$$

suggests itself. This value is in agreement with the value given by Reichardt, as indicated in section 2.5.

Figure 18 shows the variation of C_T versus y_T for another series of tests. In this series the aspect ratio was 15.8, with the outlet width $2b_0 = 0.280$ ft. The scatter of the data is wider than in the previous figure. A reasonable average for the coefficient is $C_T = 0.200$. It should be noted that for test 28 a value $C_m = 0.109$ was found for the velocity distribution, and a value of $C_T = 0.170$ approximates the coefficient for the temperature profile. This test therefore comes closer to the suggested theoretical value of C_T, than any other test in this series.

In Figure 19 the results are presented for tests 42 through 46. The scatter is seen to be rather wide and a value of $C_T = 0.220$ approximates the results. This series of tests was conducted with outlet thickness of 0.340 ft. and aspect ratio 13.4. The deviation from the theoretical value is much larger than in the previous figures.

The values

$$C_T = 0.154 \text{ with } 2b_0 = 0.115 \text{ ft.}$$
$$C_T = 0.200 \text{ with } 2b_0 = 0.280 \text{ ft.}$$
$$C_T = 0.220 \text{ with } 2b_0 = 0.340 \text{ ft.}$$

were used for calculation of the temperature profiles according to equation (2.2.1). The solid lines in Figures 6 through 10 represent equation (2.2.1) with the coefficient C_T as indicated. It is seen that these lines correlate the data reasonably well.

In general the temperature profile becomes flatter, progressing away from the outlet nozzle.

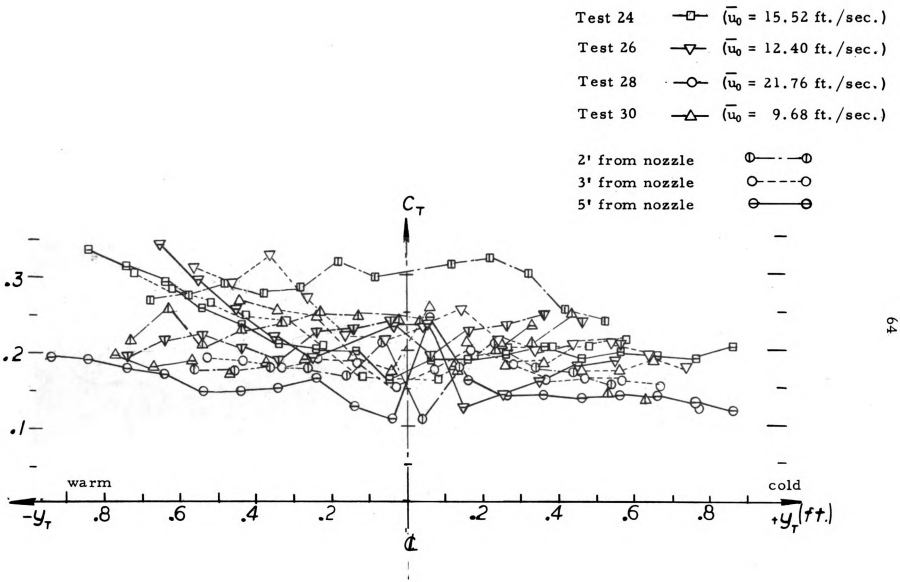

Figure 18. Plot of the coefficient C_T versus the distance y_T ($2b_0$ = 0.280 ft.).

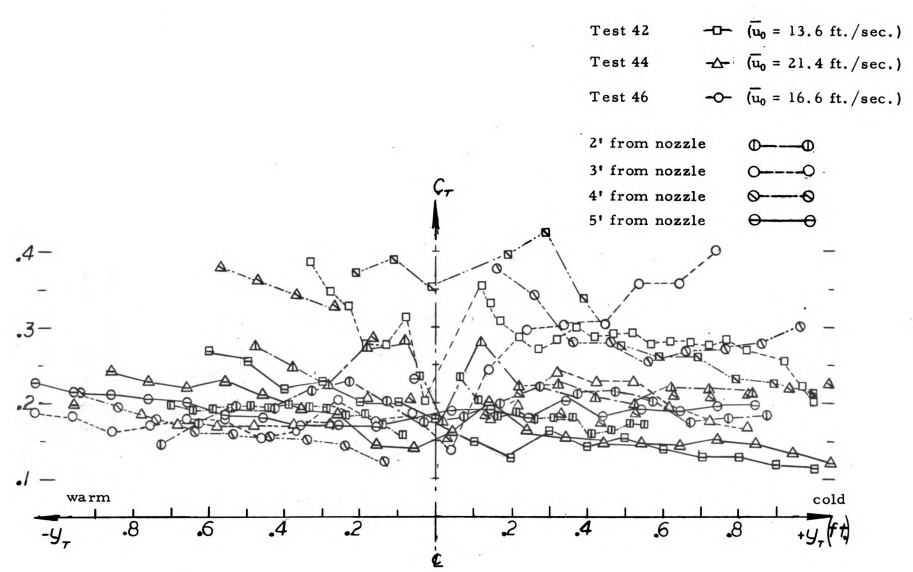

Figure 19. Plot of the coefficient C_T versus the distance y_T ($2b_0$ = 0.340 ft.).

In most cases the temperature profile and the velocity profile are assymmetric, namely, $\overline{u} = \overline{u}_m$ at $y = 0$ and $\overline{T} = \frac{1}{2}\overline{T}_m$ at $y_T = 0$ but $y \neq y_T$. In most cases the temperature profile tended to be shifted more to the warm side. However there were quite a few exceptions and no general tendency can be given here.

The effect of the temperature gradient on the apparent viscosity and the turbulence was discussed previously. It may be concluded that since the apparent viscosity ϵ_m is proportional to the temperature gradient the effect of temperature on the heat transfer is twofold, i.e., since

$$q \propto \epsilon_m \frac{dT}{dy}$$

and since

$$\epsilon_m \propto \Delta T$$

it is obvious that q will increase as some power of the temperature gradient, and this power is likely to be closer to two than to unity.

The effect of the temperature gradient on the heat transfer properties of an air curtain was not studied in detail in the present investigation, due to time and equipment limitations. This phase of the problem certainly deserves much more work, theoretical as well as experimental.

4.4 Heat Transfer Through An Air Curtain.

The results from the measurements of quantities of heat and temperatures are presented in Table 1. The results are presented in dimensionless quantities, where $Re\sqrt{\frac{H}{b_0}}$ is a parameter describing the outlet velocity and the geometry and Nu/Pr describes the overall heat transfer coefficient. To correlate the data, reference is made to section 2.3 where the semi-theoretical expression describing the heat transfer through an air curtain was derived, based on the suggested entrainment-spill mechanism.

The equation there obtained was

$$\frac{Nu}{Pr} = K\ f(a')Re\sqrt{\frac{H}{b_0}} \tag{4.4.1}$$

where the function f(a') was defined by the equation:

$$f(a') = \sqrt{\frac{C_m}{\sqrt{\pi}}} \int_{a'}^{\infty} \exp(-\eta^2)\left[1 + \operatorname{erf}\left(\frac{\eta}{\delta}\right)\right] d\eta \tag{4.4.2}$$

and where K is a constant, to be determined empirically.

The magnitude of a' can be evaluated as follows. From equation (2.6.3) and from the expression for the mass rate of flow at the outlet nozzle one gets

$$2\bar{u}_0 b_0 = Q_0 = 2 \int_0^a \bar{u}\, dy \tag{4.4.3}$$

Upon substituting equation (2.2.5) and changing variables equation (4.4.3) becomes

$$\sqrt{2}\ A\ C_m H' \int_0^{a'} \exp(-\eta^2) d\eta = b_0 \tag{4.4.4}$$

which can be further simplified to read:

$$\operatorname{erf}(a') = \sqrt{\frac{b_0}{\sqrt{\pi}\ C_m H'}} \tag{4.4.5}$$

Upon substitution of the appropriate values for b_0 and H' one gets the dimensionless width a'. For the present investigation a' was always smaller than 0.5. Therefore equation (4.4.2) was integrated numerically on a digital computer for a' ranging from zero to 0.5.

The theoretical values were substituted for the coefficients, namely $C_m = 0.109$ and $\delta = 1.414$.

The plot of f(a') versus a' is shown in Figure 20. The equation of the straight line passing through the points is the following:

$$f(a') = 0.3058 - 0.2718a' \tag{4.4.6}$$

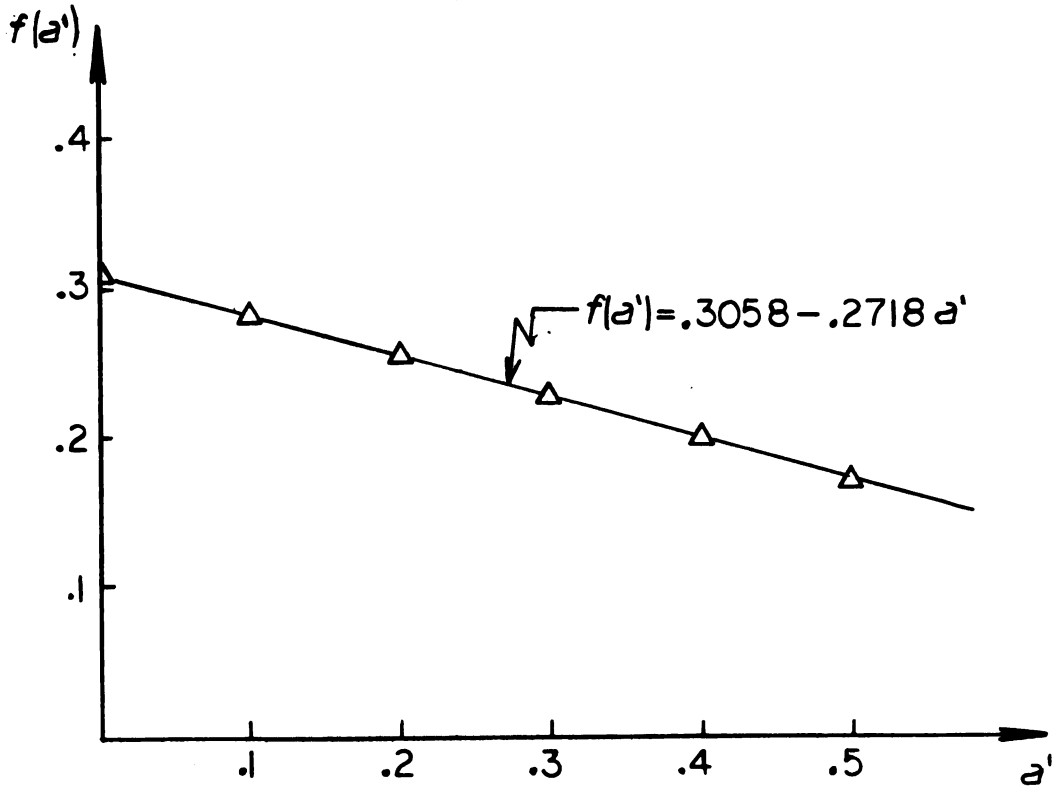

Figure 20. The function f(a') versus the dimensionless width a', as obtained from numerical integration on a digital computer.

Equation (4.4.6) can now be substituted back into equation (4.4.1) to get

$$\frac{Nu}{Pr} = K\,(0.3058 - 0.2718a')Re\sqrt{\frac{H}{b_0}} \qquad (4.4.7)$$

Since affinity of the velocity profiles was assumed, the dimensionless width a' is a function only of the geometry, namely, of the ratio H/b_0. Equation (4.4.7) can then be modified and the functional relationship determined, i.e.,

$$0.3058\ K\sqrt{\frac{H}{b_0}} - \frac{Nu}{RePr} = \phi\ (\frac{H}{b_0}) \qquad (4.4.8)$$

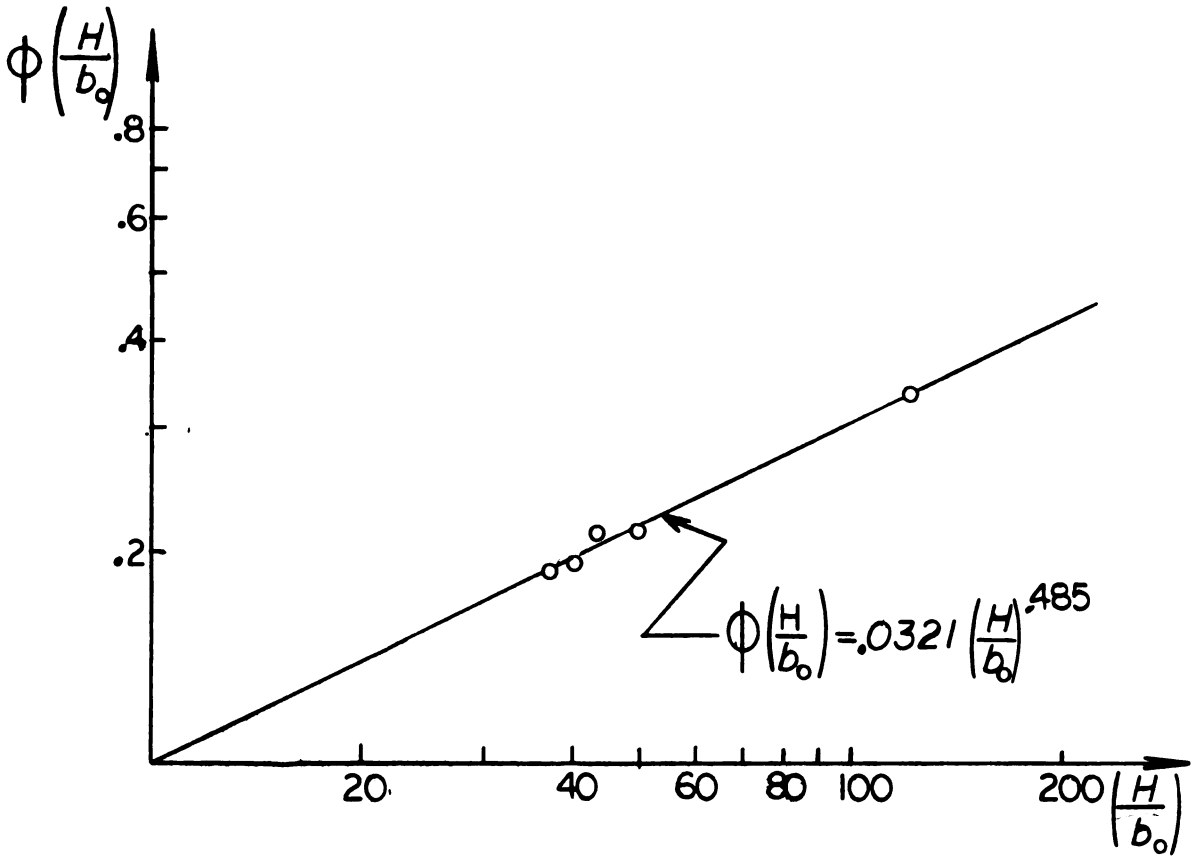

Figure 21. The function $\phi\left(\frac{H}{b_0}\right)$ versus the ratio H/b_0, on logarithmic paper.

In Figure 21 this function is plotted on a log-log paper for five values of the ratio H/b_0. For this purpose experimental data were used to calculate the ordinates, for the various values of H/b_0 encountered in the investigation. The equation of the straight line passing through the points is

$$\phi\left(\frac{H}{b_0}\right) = 0.0321\left(\frac{H}{b_0}\right)^{0.485}$$

or

$$\phi\left(\frac{H}{b_0}\right) \cong 0.0300\left(\frac{H}{b_0}\right)^{0.500} \qquad (4.4.9)$$

Upon substitution of this function $\phi\left(\frac{H}{b_0}\right)$ into equation (4.4.8) one gets the semi-theoretical expression:

$$\frac{Nu}{Pr} = 0.2758 \; K \; Re\sqrt{\frac{H}{b_0}} \qquad (4.4.10)$$

The experimental data are presented in Figure 22. These data are correlated by a straight line with a slope of 0.0808, as determined by the statistical method of least squares. These data therefore indicate that the coefficient K is:

$$K \cong 0.341 \tag{4.4.11}$$

The heat transfer through the air curtain within the experiment range of the curtain parameters $Re\sqrt{\frac{H}{b_0}}$ of 51,000 to 141,000 is expressed by the final semi-theoretical correlation

$$\frac{Nu}{Pr} = 0.0808\ Re\sqrt{\frac{H}{b_0}} \tag{4.4.12}$$

Equation (4.4.12) is accurate within ± 20 percent.

The dimensionless heat transfer for an air curtain issued at zero velocity is calculated in Appendix A.2. The value obtained is presented in Figure 22 on the ordinate. The suggested heat transfer mechanism due to the entrainment-spill process holds true only for the parameter $Re\sqrt{\frac{H}{b_0}}$ larger than approximately 50,000. For smaller values of this parameter the air curtain ceases to exist and the heat transfer is due mainly to free convection. The line describing the heat transfer in this region is probably line (b) in Figure 22. However, this region has not been studied at the present investigation.

Equation (4.4.12) can be modified as follows:

$$St_0 = 0.0808\ \sqrt{\frac{b_0}{H}} \tag{4.4.13}$$

where St_0 is the Stanton number at the outlet. This equation is also accurate within ± 20 percent for the curtain parameter $\sqrt{\frac{b_0}{H}}$ between the values 0.090 to 0.170.

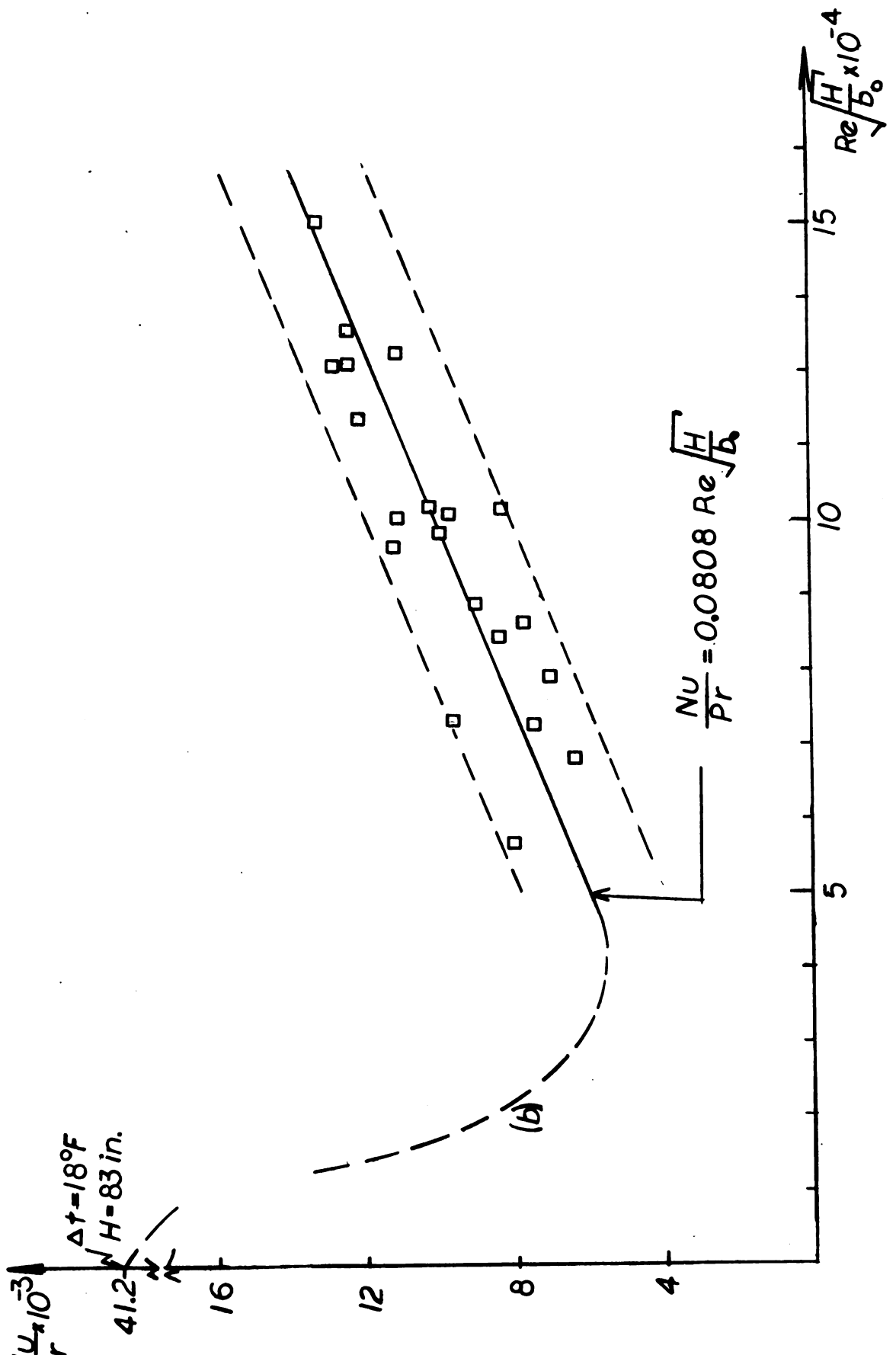

Figure 22. Experimental correlation of the dimensionless coefficient of heat transfer through an air curtain.

5. CONCLUSIONS

1. The expression suggested by Reichardt for velocity distribution in a two-dimensional jet, viz.

$$\frac{\bar{u}}{\bar{u}_m} = \exp\left(-\frac{y^2}{2C_m^2x^2}\right)$$

correlates the data reasonably well, with a coefficient of variation of 0.133. The constant C_m as suggested in the literature applies for air curtains having a product of outlet Reynolds number by the aspect ratio larger than approximately 3×10^5. For values smaller than this the C_m increases as much as 0.220.

2. The semi-theoretical distribution of the shear-stress (Figure 13) has a zero value at the centerline, at each longitudinal distance from the outlet. This profile has a maximum on each side of the centerline and drops to zero at large distances away. The magnitude of the shear stress decreases as the flow progresses away from the outlet nozzle.

The semi-theoretical value of the eddy diffusivity is found to be maximum at the centerline and close to zero at large distance away. In a substantial portion of the flow, the magnitude of this eddy diffusivity is considerably larger than that of the molecular kinematic viscosity.

3. The temperature profile in a two-dimensional jet, i.e.,

$$\frac{\bar{T}}{\bar{T}_m} = \tfrac{1}{2}\left[1 + \operatorname{erf}\left(\frac{y}{\sqrt{2}\,C_T x}\right)\right]$$

was confirmed reasonably well by experimental data. The coefficient C_T was found to be 0.154. For a three-dimensional jet, this coefficient increases as much as 0.220.

4. The experimental distribution of percent turbulence is asymmetric around the centerline of a jet subjected to unequal ambient temperatures on two sides. The intensity of turbulence on the warm side is generally much higher than that on the cold side. This may presumably be accounted for by the buoyancy forces. It appears that the higher degree of turbulence on the warm face of the jet tends to cause a shift of the jet more towards the cold side.

5. The final correlation for the heat transfer through an air curtain is found to be

$$\frac{Nu}{Pr} = 0.0808 \; Re \sqrt{\frac{H}{b_0}}$$

where the curtain parameter, $Re \sqrt{\frac{H}{b_0}}$ ranged between 57,000 and 141,000. The experimental accuracies were within the range of ± 20 percent.

APPENDIX

A.1 Equation of Motion.

The equation of motion was given in equation (2.1.3) as

$$\rho\left(\bar{u}\frac{\partial \bar{u}}{\partial x} + \bar{v}\frac{\partial \bar{u}}{\partial y}\right) = -\frac{\partial \bar{p}}{\partial x} + \frac{\partial \tau}{\partial y} \qquad (A.1.1)$$

This equation has to be satisfied by the assumed velocity profile and by expression derived for $\bar{v}$ and τ.

From equation (2.2.5)

$$\bar{u} = \bar{u}_0 A \exp(-\eta^2) \qquad (A.1.2)$$

where
$$A = \sqrt{\frac{2b_0}{\sqrt{\pi} C_m x}} \quad ; \quad \eta = \frac{y}{\sqrt{2} C_m x} \qquad (A.1.3)$$

From equation (2.2.9)

$$\bar{v} = \sqrt{2} C_m A \bar{u}_0 \left[\eta \exp(-\eta^2) - \frac{\sqrt{\pi}}{4} \operatorname{erf}(\eta)\right] \qquad (A.1.4)$$

From the first postulate

$$\frac{\partial \bar{p}}{\partial x} = 0 \qquad (A.1.5)$$

Now

$$\frac{\partial \bar{u}}{\partial x} = \left(\frac{\partial \bar{u}}{\partial A}\frac{\partial A}{\partial x} + \frac{\partial \bar{u}}{\partial \eta}\frac{\partial \eta}{\partial x}\right) = \bar{u}_0 \exp(-\eta^2)\left(-\frac{A}{2x}\right) + \left[-\bar{u}_0 A 2\eta \exp(-\eta^2)\right]\left(-\frac{\eta}{x}\right)$$

or

$$\frac{\partial \bar{u}}{\partial x} = \frac{A\bar{u}_0}{2x} \exp(-\eta^2)(4\eta^2 - 1) \qquad (A.1.6)$$

and

$$\frac{\partial \bar{u}}{\partial y} = \frac{\partial \bar{u}}{\partial \eta}\frac{\partial \eta}{\partial y} = -\frac{\sqrt{2}\,\bar{u}_0 A \eta}{C_m x} \exp(-\eta^2) \qquad (A.1.7)$$

From equation (2.3.7)

$$\tau = -\frac{\bar{u}_0^2 b_0}{\sqrt{2}\, x} \exp(-\eta^2)\, \mathrm{erf}(\eta) \qquad \text{(A.1.8)}$$

and

$$\frac{\partial \tau}{\partial y} = \frac{\bar{u}_0 b_0}{C_m x^2} \left[\eta\, \mathrm{erf}(\eta) - \exp(-\eta^2) \frac{1}{\sqrt{\pi}} \right] \exp(-\eta^2) \qquad \text{(A.1.9)}$$

Subsitution of equations (A.1.2), (A.1.4), (A.1.5), (A.1.6), (A.1.7) and (A.1.9) into equation (A.1.1) yields

$$\bar{u}_0 A \exp(-\eta^2)\left[\frac{A\bar{u}_0}{2x} \exp(-\eta^2)(4\eta^2-1) \right] + A\bar{u}_0\sqrt{2}\, C_m \left[\eta \exp(-\eta^2) - \frac{\sqrt{\pi}}{4} \mathrm{erf}(\eta)\right]$$

$$\left[-\frac{\sqrt{2}\,\bar{u}_0 A \eta}{C_m x} \exp(-\eta^2)\right] \stackrel{?}{=} \frac{\bar{u}_0^2 b_0}{C_m x^2} \left[\eta\, \mathrm{erf}(\eta) - \frac{1}{\sqrt{\pi}} \exp(-\eta^2)\right] \exp(-\eta^2) \qquad \text{(A.1.10)}$$

simplifying:

$$\frac{A^2}{2} \exp(-\eta^2)(4\eta^2-1) - \frac{A^2}{2} \left[4\eta^2 \exp(-\eta^2) - \sqrt{\pi}\, \eta\, \mathrm{erf}(\eta)\right]$$

$$\stackrel{?}{=} \frac{b_0}{C_m x} \left[\eta\, \mathrm{erf}(\eta) - \frac{1}{\sqrt{\pi}} \exp(-\eta^2) \right]$$

Substituting for A from equation (A.1.3) one gets:

$$\frac{1}{2} \frac{2b_0}{\sqrt{\pi} C_m x} \left[-\exp(-\eta^2) + \sqrt{\pi}\, \eta\, \mathrm{erf}(\eta)\right] \stackrel{?}{=} \frac{b_0}{\sqrt{\pi} C_m x} \left[\sqrt{\pi}\, \eta\, \mathrm{erf}(\eta) - \exp(-\eta^2)\right] \qquad \text{(A.1.11)}$$

This last expression is obviously an equality. Besides proving the correctness of the mathematical manipulations, equation (A.1.11) shows that the expression assumed for velocity distribution, equation (2.2.1) does satisfy the equation of motion, providing the shear stress τ is given by equation (2.3.7). This is not in itself a proof of the correctness of Reichardt's theory and hypothesis, but is a prerequisite for any assumed velocity profile or shear profile.

A.2 Free Convection Through An Opening In A Vertical Partition

The process of natural convection through an opening in a vertical partition has been studied very little.

The system under consideration is one in which two sealed chambers, at different temperatures, are separated from one another by a vertical partition having a rectangular opening of height H and width ω. Due to temperature difference a density difference will exist between the two chambers. The more dense cold air will therefore be spilled out, and warm air will be introduced into the cold chamber. An example of a case like this will be a cold enclosure, with a doorway that is not protected by an air curtain, or a doorway protected by an hypothetical air curtain issued from a slot over the doorway at zero velocity.

Assume the absolute pressure (p_0) at the elevation of the opening centerline is everywhere equal, since the density differences are small. Brown (1962) used this assumption and confirmed it experimentally.

Let the density in the cold chamber be ρ_c and that of the warm chamber be ρ_w. The pressure p at a level z below centerline will be

$$p_c = p_0 + \rho_c g z \qquad (A.2.1)$$

and in the warm chamber

$$p_w = p_0 + \rho_w g z \qquad (A.2.2)$$

The pressure difference at that level is

$$p_c - p_w = (\rho_c - \rho_w) g z \qquad (A.2.3)$$

Assuming that the air in both chambers is ideal fluid and that Bernoulli's equation applies, i.e., the velocity of flow from one chamber to the other at elevation z is

$$v = \sqrt{\frac{2g(\rho_c - \rho_w)z}{\bar{\rho}}} \qquad (A.2.4)$$

where

$$\bar{\rho} = \frac{\rho_c + \rho_w}{2} \qquad (A.2.5)$$

The mass rate of flow (Q') from one chamber to the other will be obtained by integrating equation (A.2.4) from $z = 0$ to $z = \frac{H}{2}$:

$$Q' = C \bar{\rho} \frac{\omega}{3} \sqrt{g \frac{\rho_c - \rho_w}{\bar{\rho}}} \quad H^{\frac{3}{2}} \tag{A.2.6}$$

where C is the coefficient of discharge, similar to the coefficient used in sluice-gates. The magnitude of C usually varies between 0.6 to 0.9.

The quantity of heat carried from one chamber to the other with the mass rate of flow Q' can be approximated by

$$q = Q' C_p \bar{T}_m \tag{A.2.7}$$

where

$$T_m = t_w - t_c \tag{A.2.8}$$

Define a coefficient (h_0) for the over-all heat transfer between the chambers under these conditions:

$$h_0 = \frac{q}{\omega H \bar{T}_m} \tag{A.2.9}$$

where the subscript zero stands for zero velocity of the air curtain.

In dimensionless form equation (A.2.9) with equation (A.2.7) can be written as

$$Nu = \frac{hH}{k} = \frac{C}{3} \sqrt{g \frac{(\rho_c - \rho_w)}{\nu^2 \bar{\rho}}} \quad H^3 \quad \frac{C_p \mu}{k}$$

$$= \frac{C}{3} \sqrt{Gr} \quad Pr$$

or

$$\frac{Nu}{Pr} = \frac{C}{3} \sqrt{Gr} \tag{A.2.10}$$

where the Grashof number is

$$Gr = \frac{g \Delta\rho H^3}{\bar{\rho} \nu^2}$$

Equation (A.2.10) cannot be exact because the viscosity and thermal diffusivity have been omitted. On the other hand, in heat transfer texts the Nusselt number is usually given as

$$Nu = A\,(Gr)^{a}\,(Pr)^{b} \qquad (A.2.11)$$

where A, a and b are numerical constants.

The exponent on the Pradtl number is usually close to unity and the exponent on the Grashof number is between 1/2 and 1.

Brown (1962) studied the problem of natural convection through rectangular openings in a vertical partition and suggested the equation:

$$\frac{Nu}{Pr} = 0.044\,(Gr)^{0.59} \qquad (A.2.12)$$

for the problem.

Now let the following condition exist for an air curtain issued at zero velocity:

$t_c = 65^{o}F$ $\quad \rho_c = 0.07570$ $\quad \Delta\rho = 0.00247$ (lb_m per cu.ft.)

$t_w = 83^{o}F$ $\quad \rho_w = 0.07323$ $\quad \bar{\rho} = 0.07446$ (lb_m per cu.ft.)

$\nu = 1.649 \times 10^{-4}$ (sq.ft. per sec.) for average temperature $\bar{t} = 74^{o}F$

H = 83.125 (in.) $\quad$ g = 32.174 (ft. per sq. sec.)

Then the Grashof number can be evaluated as:

$$Gr = 1.305 \times 10^{10}$$

and with this value of Grashof number equation (A.2.12) yields:

$$\frac{Nu}{Pr} = 41.2 \times 10^{3}$$

This figure is plotted in Figure 22 on the ordinate, where Re = 0.

A.3 Sample Calculations.

Test 44 will be used to demonstrate the calculations performed. In Table A.3.1 results from measurements at a distance x = 3.0 ft. from the outlet nozzle are shown.

The columns in the table are as follows:

1. Location - indicates the distance y from the jet's centerline in feet, as measured by means of the point gage.
2. Total head - indicates the reading (d) from the manometer (connected to the total head impact tube) in inches of manometer fluid.
3. Velocity head - the square root of the difference between the manometer reading (from the previous column), and the manometer reading at zero velocity (d_0 = 1.3430 in.).
4. Velocity ratio - the ratio of the velocity at any location ($\bar{u}$) to the velocity at the outlet ($\bar{u}_0$). Since the density difference is neglected this ratio is also given by the ratio of $\sqrt{d-d_0}$ at any location to $\sqrt{d-d_0}$ at the outlet.
5. Potentiometer reading, in millivolts, as obtained from the potentiometer, connected to the thermocouple on the traverse mechanism.
6. Temperature - the reading from the previous column was converted to temperature, in ^{o}F, by means of conversion tables.
7. Temperature ratio - the ratio of the temperature at any location ($\bar{t}$) subtracted from the temperature of the cold side ($\bar{t}_c$), to the maximum temperature difference across the air curtain ($\bar{T}_m$ = 14.8^{o}F) as measured at the distance x = 2.0 ft. from the outlet.
8. β - a dimensionless number , defined by equation (2.5.5), was read from Figure 16, corresponding to the temperature ratio from the previous column.
9. The distance, y_T, from the centerline of the temperature profile (y_T = 0 at $\bar{T}/\bar{T}_m = \frac{1}{2}$). This distance was measured after the points from column 7 were plotted on graph paper.
10. The coefficient C_T was calculated from the equation

$$C_T = \frac{y_T}{\sqrt{2} \times \beta}$$

where the appropriate y_T and β were substituted from previous columns.

11. Meter balance, I. The values of the hot wire anemometer's balanced circuit are given. The readings are four times milliamperes and are a measure of velocity, if a calibration curve is used. The reading at zero velocity was $I_0 = 344/4$ m.a. for this particular test.
12. Noise level, M_n. The count from the electronic counter, with an open gate for 100 seconds, was converted to r.m.s. millivolts by means of Figure 4, to obtain the noise level.
13. The root mean square voltage M_{n+v}, when the hot wire anemometer was balanced on "warm," namely, with current flowing through the hot wire.
14. The root mean square voltage, M_{n+v+s}, when the square wave was applied. The root mean square was measured by counting the frequency on the counter and converting to r.m.s. by means of Figure 4.
15. The percent turbulence was calculated from the previous columns by means of the formula:

$$\frac{\sqrt{\overline{u'^2}}}{\bar{u}} = \frac{100 \times 4 \times 3.05}{1 + \frac{B \times N}{400}} \left[\frac{I}{I^2 - I_\bullet^2} \right] \sqrt{\frac{M^2_{n+v} - M^2_n}{M^2_{n+v+s} - M^2_{n+v}}}$$

where N = 1.4 is the resistance ratio and B = 154.0 is the bridge null.

Table A.3.1. Measurements and Calculations for Test 44, x = 3.0 ft.

Location y(ft.)	Total head d(in)	Velocity head $\sqrt{d-d_0}$	$\frac{\bar{u}}{\bar{u}_0}$ (-)	Pot. Read m.v.	Temp. $\bar{t}$ ^oF	$\frac{\bar{T}}{\bar{T}_m}$ (-)	β (-)	Distance y_T(ft.)	C_T (-)	Meter Balance 4*m.a.	M_n m.v. rms	M_{n+v} m.v. rms	M_{n+v+s} m.v. rms	$\frac{\sqrt{\bar{u}'^2}}{u}$ %
.Outlet	1.4700	.356	-	0.941	74.9	-	-	-	-	445	1.64	64.9	142.6	0.565
1.0	-	-	-	0.820	69.4	.101	.895	.82	.216	-	-	-	-	-
.9	-	-	-	0.831	69.9	.135	.775	.72	.219	375	1.66	118.8	176.3	3.04
.8	1.3434	.020	.036	0.849	70.4	.169	.670	.62	.218	378	1.80	157.5	187.5	4.27
.7	1.3443	.036	.101	0.860	71.2	.223	.535	.52	.229	386	1.81	197.0	247.5	3.28
.6	1.3465	.060	.166	0.875	71.9	.270	.430	.42	.230	393	1.69	208.8	254.8	3.08
.5	1.3535	.102	.261	0.893	72.7	.324	.315	.32	.239	402	1.66	242.5	281.0	3.15
.4	1.3647	.148	.375	0.905	73.2	.356	.265	.22	.196	411	1.69	255.1	285.5	3.20
.3	1.3760	.182	.472	0.924	74.1	.419	.145	.12	.195	423	1.51	215.8	247.5	2.46
.2	1.3850	.208	.527	0.943	75.0	.480	.035	.02	.135	426	1.59	228.0	277.0	1.94
.1	1.3885	.214	.543	0.973	76.3	.567	.135	.08	.140	426	1.70	218.8	264.1	1.98
0.0	1.3876	.212	.536	0.990	77.0	.615	.205	.18	.207	428	1.73	232.6	269.3	2.24
.1	1.3855	.206	.524	1.020	78.3	.704	.385	.28	.171	419	1.67	230.6	275.2	2.21
.2	1.3760	.182	.462	1.040	79.3	.771	.520	.38	.172	411	1.58	257.0	294.5	2.88
.3	1.3627	.140	.357	1.060	80.1	.825	.655	.48	.173	407	1.62	267.3	317.5	2.66
.4	1.3500	.084	.235	1.076	80.8	.873	.800	.58	.171	398	1.74	271.3	302.5	4.01
.5	1.3450	.045	.126	1.085	81.2	.906	.925	.68	.173	389	1.74	239.5	269.0	4.57
.6	1.3435	.022	.048	1.090	81.5	.920	.980	.78	.187	383	1.71	182.0	224.0	3.73
.7	-	-	-	-	-	-	-	-	-	371	1.67	149.7	194.3	4.60

In Table A.3.2 the results of measurements in quantities of heat and temperatures are given. The columns of this table are as follows:

1. The date and time for each test.
2. The duration of each test, in hours.
3. The amount of energy required to maintain the warm chamber at constant temperature in Btu per hr.
4. The heat losses through the walls, q_e. The losses were determined by the calibration of the warm chamber to be 89.2 Btu per hr., ^{o}F. The temperature difference between the warm chamber and the outside was multiplied by this figure to obtain the heat losses in Btu per hr.
5. The net quantity of heat transferred through the air curtain, q, is given in Btu per hr. This quantity was found by subtracting q_e from q_1, i.e.,
$$q = q_1 - q_e.$$
6. The average temperature at the warm side, t_w. All the hourly recordings from the thermocouples in the warm side were averaged for the test period.
7. The average temperature of the cold side, t_c, obtained by similar procedure.
8. The temperature gradient across the air curtain is defined by $\Delta t_1 = t_w - t_c$.
9. The outside temperature, t_0, an average of hourly recordings of two thermocouples located outside of the warm chamber, in ^{o}F.
10. The temperature difference between the warm chamber and the outside, i.e.,
$$\Delta t_2 = t_w - t_0.$$
11. The overall heat transfer coefficient through the air curtain, in Btu per hr., ^{o}F, sq. ft. The quantity of heat q is divided by the area of the doorway ($A = 52\frac{1}{2} \times 83\frac{1}{8}/144 = 30.3$ sq. ft.), and by the temperature difference existing across the air curtain, Δt_1.

Table A.3.2. Heat and Temperature Measurements for Test 44.

Date and Time	Time hrs.	Heat (Btu/hr)			Temperature (^{o}F)					$\frac{\text{Btu}}{\text{hr } ^{o}\text{F sq. ft.}}$
		q_1	q_e	q	t_w	t_c	Δt_1	t_0	Δt_2	h
Dec. 7, 12:25 - Dec. 7, 23:30	10.083	11,543	3,960	7,573	80.3	68.0	12.3	35.8	44.5	20.32
Dec. 7, 23:30 - Dec. 8, 10:50	12.333	12,010	4,157	7,853	81.2	68.9	12.3	34.6	46.6	21.07
Dec. 9, 00:50 - Dec. 9, 09:20	8.500	11,925	5,138	6,787	82.8	71.2	11.6	25.2	57.6	19.31
Dec. 9, 12:30 - Dec. 9, 23:30	11.000	11,666	4,674	6,992	81.8	70.2	11.6	29.4	52.4	19.89
Dec. 9, 23:30 - Dec. 10, 09:00	9.500	12,179	5,477	6,702	83.5	71.7	11.8	22.1	61.4	18.75
Dec. 10, 09:00 - Dec. 10, 23:00	14.000	11,824	5,209	6,615	80.8	70.0	10.8	22.4	58.4	20.21
Dec. 10, 23:00 - Dec. 11, 09:05	10.083	12,253	5,736	6,517	76.9	66.4	10.5	12.6	64.3	20.49

Remark: The heat losses through the walls were determined by calibrating the warm chamber. Seven tests were run for calibration. The amount of heat lost through the walls was, with a level of significance of 95 percent, $q_e = 89.2 \pm 2.33$ Btu per hr, ^{o}F.

In addition a dimensionless number describing the heat transferred through the air curtain was calculated, namely

$$\frac{Nu}{Pr} = \frac{\bar{h}\, H}{\rho\, C_p\, \nu}$$

where the overall heat transfer coefficient $\bar{h}$ is the average of the values presented in column 12.

The properties of the air were obtained from the International Critical Tables, for the temperature of the air at the outlet (t_a). For this test $t_a = 73.6\ ^{o}F$ therefore $\rho = .0745$ lb per cu. ft., $\nu = 1.647 \times 10^{-4}$ sq. ft. per sec. and $C_p = 0.24$ Btu per lb, ^{o}F.

The velocity of the air at the outlet, for this test, was calculated from the equation

$$\bar{u}_0 = \sqrt{\frac{2g}{12} \frac{\gamma_m}{\rho} (d-d_0)}$$

where $\gamma_m = 50.55\ lb_m$ per cu. ft. is the density of the manometer fluid, obtained from the International Critical Tables for the appropriate temperature. Substituting the proper values

$$\bar{u}_0 = 2.315 \sqrt{\frac{50.55}{.0745}} \times 0.356$$

or

$$\bar{u}_0 = 21.35 \text{ ft. per sec.}$$

and the outlet Reynolds number

$$Re = \frac{\bar{u}_0\, b_0}{\nu} = \frac{21.35 \times 0.170}{1.647 \times 10^{-4}}$$

$$Re = 22,000$$

Finally

$$Re \sqrt{\frac{H}{b_0}} = 22,000 \sqrt{\frac{83.125}{12 \times 0.170}} = 140,710$$

REFERENCES

Abramovitch, G.
1939. The theory of a free jet of a compressible gas.
NACA TN 1058.

Albertson, M. L.; Dai, Y. B.; Jensen, R. A. and Rouse, H.
1950. Diffusion of submerged jets.
Trans. ASCE 115: 639-697.

Alexander, L. G. et al.
1953. Transport of momentum, mass and heat in turbulent jet.
Univ. of Ill. Eng. Exp. Stat. Bull. No. 413.

American Society of Mechanical Engineers Research Publication
1937. Fluid Meters, Their Theory and Application.
4th edition.

Bickley, W. G.
1937. The plane jet.
Phil. Mag. 23:727-731.

Birkhoff, G.
1957. Jets, Wakes and Cavities.
Academic Press Inc., N. Y.

Bjorkman, R. V.
1961. Air curtain improves plant heating.
Air Eng. January.

Boussinesq, J.
1877. Essai sur la theorie des eaux courantes.
Memoires presentes par divers savants a l'Academie des Sciences 23.

Brown, W. G. and Solvason, K. R.
1962. Natural convection through rectangular openings in partitions-1
Int. J. Heat Mass Transfer, 5:859-868.

Cadiergues, R.
1957. Warm air curtains.
Heating and Ventilating and Journal of Air Conditioning, 30:423.

Callaghan, E. E. et al.
1949. Investigation of flow coefficient of circular, square and elliptical orifices at high pressure ratios.
NACA TN 1947.

Chia-Chiao Lin
1947. Velocity and temperature distributions in turbulent jets.
The Science Repts. of National Tsing Hua Univ.
4(5):419-450.

Chou, P. Y.
1947. The laminar mixing motion of two incompressible gases.
Chinese Journal of Physics, China, Vol. 7, p. 96.

Cleeves, V.
1947. Isothermal and nonisothermal air-jet investigation.
Chem. Eng. Progress, 43(3):123-134, March.

Corrsin, S.
1949. Extended applications of the hot wire anemometer.
NACA TN 1864.

Corrsin, S.
1949. Diffusion of submerged jets: Discussion.
A.S.C.E. 75:901.

Corrsin, S. et al.
1950. Further experiments in the flow and heat transfer in a heated turbulent air jet.
NACA Rept. 998.

Corrsin, S. and Kistler, A. L.
1954. The free stream boundaries of turbulent flows.
NACA TN 3133; January.

Eckert, E. R. G. and Drake, R. M.
1959. Heat and Mass Transfer.
McGraw Hill Book Co., N. Y.

Elrod, H. G.
1954. Computation charts and theory for rectangular and circular jets.
Trans. ASHVE 60:431-444.

Ferrari, C.
1935. The transport of vorticity through fluids in turbulent motion.
NACA TM 799.

Flow Corporation.
1958. Model HWB2 hot wire anemometer theory and instruction.
Flow Corp. Bulletin No. 37B.

Forstall, W. and Shapiro, A. H.
1950. Momentum and mass transfer in coaxial gas jets.
ASME Jr. of Appl. Mech. 72:399-408.

Forthmann, E.
1936. Turbulent jet expansion.
NACA TM 789.

Görtler, H.
1942. Berechnung von Aufgaben den freien Turbulenz auf Grund eines neuen Näherungsansatzes.
ZAMM 22(5):244-254.

Gygax, E. E.
1956. Air curtain seals door opening.
Heating, Piping and Air Conditioning, 28(1):146-147.

Gygax, E. E.
1957. Air curtain entrances grow wider.
Heating, Piping and Air Conditioning 29(10):124-126.

Helander, L. et al.
1954. Characteristics of downward jets of heated air from a vertical discharge unit heater.
Trans. ASHVE 60:359-384.

Hetsroni, G.
1961. Heat transfer through an air curtain.
Unpublished thesis for M.S. degree, Michigan State Univ., East Lansing, Michigan.

Hinze, J. O. et al.
1948. Transfer of heat and matter in the turbulent mixing zone of an axially symmetrical jet.
Appl. Sci. Res. A-1, 435-461.

Howarth, L.
1938. Distribution in plane and axially symmetrical homogeneous jets.
Proc. Cambridge Phil. Soc. 34:185.

Hukill, W. V. and Smith, E.
1946. Cold storage for apples and pears.
USDA Cir. No. 740.

Kármán, T. von and Howarth, L.
1938. On the statistical theory of isotropic turbulence.
Proc. Roy. Soc., London, ser. A 164 (914):192-215.

Koestel, A.
1954. Computing temperatures and velocities in vertical jets of hot or cold air.
Trans. ASHVE 60:385-410.

Kuethe, A. M.
1935. Investigations of the turbulent mixing regions formed by jets.
Journ. Appl. Mech. 2, A87-95.

Kurek, E. J.
1962. All about air entrances.
Air Eng. 4(6):38-42 June, 62; 39-40 July, 62.

Liepmann, H. W. and Laufer, J.
1947. Investigation of free turbulent mixing.
NACA TN 1257.

Lin, C. C.
1947. Velocity and temperature distributions in turbulent jets.
The Science Reports of National Tsing Hua Univ.
series A, vol. 4, October.

Loitsianskii, L. G.
1944. Integral methods in the theory of the boundary layer.
NACA TM No. 1070.

Michael, W. R.
1960. Luftschleiertüren fur Kühlraume.
Die Kälte 13(12):679-682.

Milne-Thomson, L. M.
1955. Theoretical Hydrodynamics.
The Macmillan Co., N. Y.

Norton, W.
1959. Where to use a curtain of air.
Consulting Engineer 11(3):108-113.

Pai, Shih-J.
1954. Fluid Dynamics of Jets.
D. van Nostrand Co. Inc., N. Y.

Pai, S. I.
1955. On turbulent mixing of two cases at constant temperature.
Journ. Appl. Mech. 22, 41-47.

Patchen, G. O.
1961. Air door for cold storage houses.
USDA AMS Bull. No. 458.

Prandtl, L.
1925. Berichte uber Untersuchungen zur ausgebildeten Turbulenz.
ZAMM 5:125.

Prandtl, L.
1926. Ueber die ausgebildete Turbulenz.
Verhandlungen des-2 Internahonalen Kongresses für
Technische Mechanik. Zurich (1926), pp. 62-74.

Prandtl, L.
1942. Bermerkungen zur Theorie der freien Turbulenz.
ZAMM 22(5):241-243.

Reichardt, H.
1941. Uber eine neue Theorie der freien Turbulenz.
ZAMM 21(5):257-264.

Reichardt, H.
1942. Gesetzmäsigkeiten der frein Turbulenz.
VDI- Forsch., 414.

Reichardt, H.
1944. Impuls-und Warmeaustausch in freier Turbulenz.
ZAMM 24, 268.

Ricou, F. P. et al.
1961. Measurements of entrainment by axisymmetrical turbulent jet.
Jr. of Fluid Mechanics 11(1):21-32 Aug.

Rouse, H.
1959. Advanced Mechanics of Fluids.
J. Wiley and Sons, N. Y.

Ruggeri, R. S. et al.
1950. Penetration of air jets issuing from circular, square and elliptical orifices directed perpendicular to an air stream.
NACA TN 2019.

Schlichting, H.
1933. Laminare Strahlausbreitung.
ZAMM 13:260.

Schlichting, H.
1960. Boundary Layer Theory.
McGraw Hill Book Co.; N. Y.

Schmidt, W.
1941. Turbulente Ausbreitung eines Stromes erhitzter Luft.
ZAMM 21:265-278.

Seban, R. A. et al.
1962. Velocity and temperature profiles in turbulent boundary layers with tengential injection.
Jr. of H. T. Trans. ASME 84(1):45-54, February.

Sleight, P.
1961. Curtains of air.
Compressed Air Mag. 66(10):15-17, October.

Squire, H. B.
1948. Reconsideration of the theory of free turbulence.
Phil. Mag. 39:1-20; Jan.

Steiner, E.
1958. Device for producing a room-closing air curtain.
U. S. Patent No. 2, 863, 373.

Szablewski, W.
1950. The diffusion of a hot air jet in air in motion.
NACA TM 1288.

Taylor, G. I.
1935. Statistical theory of turbulence.
Proc. Roy. Soc., London, ser. A 151 (873).

Taylor, G. I.
1937. Transport of vorticity and heat through fluids in turbulent motion.
Proc. Roy. Soc. 135A, 685.

Tollmien, W.
1926. Calculation of turbulent expansion processes.
ZAMM 6:468-478.

Williams, R. M.
1958. Refrigeration losses through open doors and conveyor passes.
Unpublished thesis for M. S. degree, Michigan State Univ.,
East Lansing, Michigan.